



DE05FF048

GSF-Bericht 02/05

Photon Dose Conversion Coefficients for the Human Teeth in Standard Irradiation Geometries

A. Ulanovsky, A. Wieser, M. Zankl, P. Jacob

Institut für Strahlenschutz

GSF—Forschungszentrum für Umwelt und Gesundheit, GmbH

Ingolstädter Landstraße 1, D-85764, Neuherberg



GSF—National Research Center
for Environment and Health
member of the Helmholtz Association

Herausgeber:

**GSF - Forschungszentrum
für Umwelt und Gesundheit, GmbH**

Ingolstädter Landstraße 1
D-85764 Neuherberg

Telefon 089/3187 - 0
Telefax 089/3187 - 3372
Internet <http://www.gsf.de>

Mitglied der Hermann von Helmholtz-Gemeinschaft
Deutscher Forschungszentren (HGF)

© GSF-Forschungszentrum, 2005

ISSN 0721 - 1694

Gedruckt auf umweltfreundlichem, chlorfrei gebleichtem Papier



Abstract — photon dose conversion coefficients for the human tooth materials are computed in energy range from 0.01 to 10 MeV by the Monte Carlo method. The voxel phantom Golem of the human body with newly defined tooth region and a modified version of the EGS4 code have been used to compute the coefficients for 30 tooth cells with different locations and materials. The dose responses are calculated for cells representing buccal and lingual enamel layers. The computed coefficients demonstrate a strong dependence on energy and geometry of the radiation source and a weaker dependence on location of the enamel voxels. For isotropic and rotational radiation fields the enamel dose does not show a significant dependence on tooth sample locations. The computed coefficients are used to convert from absorbed dose in teeth to organ dose or to integral air kerma. Examples of integral conversion factors from enamel dose to air kerma are given for several photon fluences specific for the Mayak reprocessing plant in Russia. The integral conversion factors are strongly affected by the energy and angular distributions of photon fluence, which are important characteristics of an exposure scenario for reconstruction of individual occupational doses.

Contents

1. Introduction	11
2. Materials and Methods	13
2.1. Dose conversion coefficients	13
2.2. Description of phantom	15
2.3. Simulation technique	17
2.4. Description of the variance reduction technique	18
2.5. Scoring	22
3. Results	25
3.1. Dose conversion coefficients for tooth enamel	25
3.2. Simulation of coupled electron-photon transport	29
4. Discussion	41
4.1. Comparison with other calculated data	41
4.2. Integral enamel dose and air kerma for occupational exposure scenarios	42
5. Conclusions	49
A. Appendix	57

Contents

List of Tables

2.1. Compositions of tooth materials based on data from ICRP Publication 23 [12].	16
3.1. Jaw-averaged enamel DCCs, $C_{k,T}$, for the AP-geometry at different locations. Shown in the brackets are values of the coefficient of variation (CV).	30
3.2. Jaw-averaged enamel DCCs, $C_{k,T}$, for the PA-geometry at different locations. Shown in the brackets are values of the coefficient of variation (CV).	31
3.3. Jaw-averaged enamel DCCs, $C_{k,T}$, for the LLAT-geometry at different locations. Shown in the brackets are values of the coefficient of variation (CV).	32
3.4. Jaw-averaged enamel DCCs, $C_{k,T}$, for the RLAT-geometry at different locations. Shown in the brackets are values of the coefficient of variation (CV).	33
3.5. Jaw-averaged enamel DCCs, $C_{k,T}$, for the TOP-geometry at different locations. Shown in the brackets are values of the coefficient of variation (CV).	34
3.6. Jaw-averaged enamel DCCs, $C_{k,T}$, for the CC-geometry at different locations. Shown in the brackets are values of the coefficient of variation (CV).	35
3.7. Jaw-averaged enamel DCCs, $C_{k,T}$, for the ROT-geometry at different locations. Shown in the brackets are values of the coefficient of variation (CV).	36

List of Tables

3.8. Jaw-averaged enamel DCCs, $C_{k,T}$, for the ISO-geometry at different locations. Shown in the brackets are values of the coefficient of variation (CV). 37

3.9. Ratio of dose conversion coefficients for enamel and dentine computed without electron transport (kerma approximation) and with electron transport and electron energy cut-off equal to 10 keV. The data shown are for the «Front» tooth location under AP irradiation geometry. Shown uncertainties represent 2σ statistical errors. 39

4.1. Ratio of absorbed dose in the different enamel layers and integral air kerma for various photon spectra and different tooth segments. 44

List of Figures

2.1. Slice of the "Golem" phantom head showing tooth cells and their separation into five locations: (1) Front, (2) Front-Left, (3) Front-Right, (4) Left, and (5) Right. Also indicated are: (6) bone, (7) spine and spinal cord, (8) trachea, and (9) soft tissues.	23
2.2. Illustration of the source importance sampling for arbitrary spatial coordinate u . Shown are univariate normalized Cauchy (solid line) and uniform (dashed line) probability density distributions. .	24
3.1. Dose conversion coefficients for tooth enamel in the upper and lower jaws. The coefficients are averaged over locations and buccal/lingual layers. Closed symbols – TOP source; open symbols – CC source.	27
3.2. Tooth enamel dose conversion coefficients for different locations/layers in AP irradiation geometry. The coefficients are averaged over upper and lower jaws. Closed symbols — location «Front»; open symbols — location «Left».	28
3.3. Tooth enamel dose conversion coefficients for different locations/layers in ROT irradiation geometry. The coefficients are averaged over upper and lower jaws. Closed symbols location — «Front»; open symbols — location «Left».	38

List of Figures

4.1. Comparison of the dose conversion coefficients of the present study – open symbols, dashed line – for tooth enamel in AP irradiation geometry with those of Takahashi <i>et al.</i> [5] – closed symbols. Location «Front-Left» corresponds to location «Middle» in Takahashi <i>et al.</i> [5].	46
4.2. Comparison of the dose conversion coefficients of the present study – open symbols, dashed line – for tooth enamel in PA irradiation geometry with those of Takahashi <i>et al.</i> [5] – closed symbols. Location «Front-Left» corresponds to location «Middle» in Takahashi <i>et al.</i> [5].	47
A.1. Screenshot of the utility in the operation mode «Plot».	58
A.2. Screenshot of the utility in the operation mode «Compute».	60
A.3. An additional window showing use-defined energy distribution of fluence. Shown is the A80 X-ray spectrum [22]. Options selected are: «x-log», «y-lin», and «spline interpolation».	61

1. Introduction

Electron paramagnetic resonance (EPR) spectrometry of the human tooth enamel is recognized as a valuable method for reconstructing the dose to individuals [1, 2]. The EPR-spectrometry methods are capable of assessing the absorbed dose in a given tooth sample. To convert this dose to an organ dose or to air kerma, it is necessary to have appropriate dose conversion coefficients (DCC). Such coefficients are known to depend on type, energy, and angular properties of the incident radiations as well as on the type and location of the given tooth sample. The dose coefficients for the human tooth enamel were investigated both experimentally and by Monte Carlo method by Wieser *et al.* [3]. Human teeth (molars) in a physical head-sized Plexiglas phantom were irradiated by low-energy X-rays and ^{60}Co gamma-rays and absorbed doses in the enamel were determined by EPR-method. The experiments were also simulated by Monte Carlo method and a good agreement was found between the calculated and measured values. However, neither the phantom itself nor the location of a tooth sample inside the phantom was realistic.

Takahashi *et al.* [4, 5, 6] used mathematical and voxel phantoms to calculate absorbed doses in human teeth due to external photon irradiation. Computations were performed for eight photon energy values between 0.03 and 2.5 MeV. No electron transport was simulated, i.e. all the calculations had been performed in kerma-approximation. The photon sources considered by Takahashi *et al.* were parallel beams on the sides of the phantoms (excluding top and bottom sides). The response for the rotational exposure geometry was approximated by averaging dose responses for parallel beams incident from different angles.

Takahashi *et al.* calculated the dose responses for five tooth regions; however, the teeth were not separated into enamel and dentine. Instead, they have

1. Introduction

calculated average tooth dose responses and obtained enamel dose responses using a rescaling technique. Such procedure seems to be insufficient, because for EPR-measurements the tooth enamel is primarily used. The rescaling of the average tooth dose does not provide information on differences between the dose absorbed in the buccal and lingual parts of tooth enamel.

Tooth doses measured by EPR-method can be converted to organ or effective dose for a given individual. Current tabulation of the DCCs (organ and effective dose per air kerma) in the ICRP Publication 74 [7] covers the energy range from 10 keV to 10 MeV for six irradiation geometries. Therefore, to convert the tooth enamel dose responses to the organ or effective doses the energy range and irradiation geometries must be consistent.

In the present work a voxel phantom of the human body [8] has been used to calculate doses in tooth enamel (buccal and lingual) and dentine for photon radiation. Photon sources are considered in eight irradiation geometries and the photon energies cover a range from 10 keV to 10 MeV corresponding to the energy scale of organ DCCs from [7]. Computation of the DCCs for the high energy photons (up to 10 MeV) required accounting for coupled electron-photon transport in the Monte Carlo calculations.

The report describes the computational procedure and presents calculated DCCs for the human teeth as a function of irradiation geometries and incident photon energies for different materials (buccal and lingual enamel and dentine) and locations in the mouth. To facilitate visualization, processing and conversion of the numerous dose conversion coefficients, a special-purpose software utility has been developed and used. Information on the utility is given in Appendix.

The report demonstrates application of the conversion coefficients for reconstruction of integral air kerma at several workplaces at «Mayak» facility in Russia [9] and for evaluation of the human effective and organ doses.

2. Materials and Methods

2.1. Dose conversion coefficients

The current report deals with radiation sources regarded as standard in radiation protection practice [7]. The standard sources have pre-defined angular properties of the emitted radiations (source geometry) and dose responses to such sources are specific for the given geometries. The present study is limited to photon sources.

Consider monoenergy ($E = E_0$) photon source with pre-defined exposure geometry, irradiating a target object¹. If the target does not disturb the radiation field then the photon fluence, Φ , created by the source is uniform and independent on spatial co-ordinates

$$\Phi(\vec{r}, E_0) = \Phi(E_0).$$

A dose conversion coefficient can be defined in different ways. One definition, which is more convenient in radiation transport calculations, expresses the dose coefficient as absorbed dose in a target object, $D(E_0)$, per source particle fluence, $\Phi(E_0)$:

$$C_f(E_0) = \frac{D(E_0)}{\Phi(E_0)}, \quad (2.1)$$

where index f indicates the coefficient is defined through the fluence. The dose, given an arbitrary energy distribution of fluence, is given as

$$D = \int_E C_f(E) \Phi(E) dE \quad (2.2)$$

¹Under the target object we assume any object of dosimetry interest, like a human body, a specific organ, or even a ceramic tile or a brick.

2. Materials and Methods

or, if the fluence rate, $\phi(E, t) = \frac{d\Phi(E)}{dt}$, and coefficients, $C_f(E, t)$, are not stationary, as

$$D = \int_T \int_E C_f(E, t) \phi(E, t) dE dt. \quad (2.3)$$

In the present study, however, the dose conversion coefficients are considered time-independent as applicable to occupational exposure of adult professionals. Thus, in this particular case the Eqn. (2.3) reduces to the Eqn. (2.2).

Assessment of the incident particle fluence is straightforward in radiation transport calculations by Monte Carlo method. However, in most practical applications radiation sources cannot be assumed monoenergetic and the fluence of source particles is not directly measured. It is usual in practice that only integral quantities, like exposure or absorbed dose in air, are measured. That is, Eqn. (2.1) has to be redefined to include the quantities used in practice.

Taking into account definition of photon kerma free-in-air (see e.g. Section A.2.1 of ICRU Publication 47[10])

$$K_a(E_0) = \left(\frac{\mu_{tr}}{\rho}(E_0) E_0 \right) \Phi(E_0) = k_{tr}(E_0) \Phi(E_0) \quad (2.4)$$

where $\frac{\mu_{tr}}{\rho}(E_0)$ is a mass-energy transfer factor (cm^2g^{-1}), then the fluence for monoenergetic radiation can be expressed via air kerma

$$\Phi(E_0) = \frac{K_a(E_0)}{k_{tr}(E_0)}. \quad (2.5)$$

Substituting now Eqn. (2.5) into Eqn. (2.1), one obtains

$$C_f(E_0) = k_{tr}(E_0) C_k(E_0) \quad (2.6)$$

where

$$C_k(E_0) = \frac{D(E_0)}{K_a(E_0)} \quad (2.7)$$

is a definition of dose conversion coefficients for external irradiation adopted by ICRP [7]. Index k indicates kerma-based definition of the dose coefficients.

The above equations are given for monoenergy photons. Consider now

2.2. Description of phantom

energy-integrated quantities: kerma free-in-air, K_a , absorbed dose in an organ of the human body, D_G , and absorbed dose for the tooth enamel, D_T . For arbitrary energy distribution of fluence, $\Phi(E)$, it follows from the Eqs. (2.2), (2.4), and (2.6):

$$K_a = \int_E k_{tr}(E')\Phi(E')dE' \quad (2.8)$$

$$D_T = \int_E C_{k,T}(E')k_{tr}(E')\Phi(E')dE' \quad (2.9)$$

$$D_G = \int_E C_{k,G}(E')k_{tr}(E')\Phi(E')dE' \quad (2.10)$$

where $C_{k,T}(E)$ and $C_{k,G}(E)$ are kerma-based energy-dependent dose conversion coefficients for the tooth enamel and the organ, respectively.

To calculate using the above equations one gets the values of $k_{tr}(E)$ from tabulated mass-energy transfer factors (see e.g. [10] and [11]), the values of $C_{k,G}(E)$ — from [7]. The energy spectrum of incident radiation, $\Phi(E)$, and irradiation geometry (i.e. angular properties of the source) are problem-specific characteristics and have to be determined or implied depending on the specific dose reconstruction problem. The only missing are the values of $C_{k,T}(E)$, which are calculated in the current study and presented in this report.

2.2. Description of phantom

The phantom used for calculation of the DCCs in the human teeth, Golem, is a voxel phantom of the human body [8]. The phantom is described in terms of small rectangular volumes — voxels. Every voxel has a dimension of $0.208 \times 0.208 \times 0.8 \text{ cm}^3$. Because of the rectangular geometry, a surface bounding the phantom has also the shape of a box (rectangular prism). The phantom in its original version [8] had the teeth implemented as one region (material — hard bone with density of 1.92 g cm^{-3}).

For the purposes of the current study, the tooth region has been further modified. The tooth region has been split into 30 sub-regions in order to achieve a higher detailing. These sub-regions are grouped into two slices, rep-

2. Materials and Methods

representing upper and lower jaws, each having five segments of the tooth arc. Every segment is divided into three layers representing buccal enamel, dentine, and lingual enamel. New materials have been introduced in the phantom description: enamel ($\rho = 2.92 \text{ g cm}^{-3}$) and dentine ($\rho = 2.51 \text{ g cm}^{-3}$). The elemental composition of these materials has been selected in accordance with ICRP Publication 23 [12] and is shown in Table 2.1.

Table 2.1.: Compositions of tooth materials based on data from ICRP Publication 23 [12].

Material	ρ (g cm^{-3})	Element weight fraction (%)						
		H	C	N	O	Mg	P	Ca
Enamel	2.92	0.41	0.64	0.20	43.40	0.32	18.00	37.00
Dentine	2.51	1.50	2.80	0.88	47.40	0.78	15.20	31.20

The phantom head slice with the lower jaw is shown in Fig. 2.1. In the figure, the tooth segments are numbered from (1) to (5). In each segment, the voxels of lighter gray tone indicate enamel layers (both buccal and lingual).

The Monte Carlo simulations have been performed with a customized version of the widely-known code EGS4 [13]. The standard EGS4 distribution² with the PRESTA algorithm [14] was combined with the routines describing the voxel phantom geometry and dose scoring routines [15]. For the purpose of the present study, the program has been further modified:

- the tooth region, as already mentioned, is split into 30 cells and new materials (enamel and dentine) replaced the old teeth material,
- the source sampling routine is extended to encompass the full range of the standard irradiation geometries (see [7]), and
- source importance sampling as a variance reduction technique is implemented.

²www.slac.stanford.edu/egs/codes/zip/egs4pc.zip

2.3. Simulation technique

The principal goal of the study is to compute energy-dependent dose conversion coefficients, $C_{k,T}(E)$ (see Eqs. (2.7) and (2.9)), for the human teeth enamel as a function of a tooth location for a number of standard radiation fields. These standard fields are:

- antero-posterior (AP),
- postero-anterior (PA),
- left lateral (LLAT),
- right lateral (RLAT),
- caudo-cranial (CC),
- cranio-caudal (TOP),
- rotational (ROT), and
- isotropic (ISO).

First six fields are planar monodirectional photon beams, coming from one specific side of the phantom's box. The last two fields (ROT and ISO) represent isotropic fields in the horizontal (x, y) -plane and in space, respectively. The rotational (ROT) source is regarded as relevant to many cases of occupational exposure.

The source sampling has been performed on the surface of a box (rectangular prism) around the phantom. Each planar monodirectional source is sampled on a corresponding face of the box. Starting locations for the ROT source are sampled on the four vertical faces of the box, and the total box surface is used to sample the ISO source; thus the source areas are ranging from 0.14 m^2 (CC and TOP sources) to 2.08 m^2 (ISO source). At the same time, the target regions – the tooth enamel cells – have very small volumes ranging from 0.21 cm^3 to 0.73 cm^3 . For such small volumes a probability for a

2. Materials and Methods

source particle to hit a region of interest is also very small and a direct analog simulation of the radiation transport is computationally inefficient: most of the source particles do not contribute to the dose estimate. Consequently, the Golem phantom related code has been modified to allow the following: (a) sampling of the ISO- and ROT-source on the surface of a box around of the phantom (sampling on a sphere around the phantom would be evidently less computationally efficient), and (b) positional biasing of the source particles to implement importance sampling (see next Section) for all geometries.

Calculations have been performed for 18 photon energy values in range from 10 *keV* to 10 *MeV*. Photons were followed in the simulations until their energies were degraded below 3 *keV*. Several values for terminating the tracking of secondary electrons were investigated and the value of 100 *keV* was found to be adequate for present simulations. Maximum linear range in the enamel and in the dentine for the electrons with energy 100 *keV* is between 0.062 *mm* and 0.071 *mm*. These values are approximately 3.5% of the smallest dimension of a voxel in the Golem phantom. That is, electron leakage from the tooth voxels does not affect the average dose value in the voxel. Moreover, because of the tooth voxels are surrounded by soft tissue voxels the electrons coming from the latter compensate for electrons leaking from the former. In fact, noticeable differences between calculations done with and without electron transport appear at the source photon energies higher than 3 *MeV* (see Table 3.9 in the Chapter 3).

2.4. Description of the variance reduction technique

As it is mentioned in the previous section, the teeth enamel target cells have volumes ranging from 0.21 *cm*³ to 0.73 *cm*³, thus a direct analog simulation of coupled electron and photon transport is not efficient computationally. To achieve acceptable statistical uncertainties of the Monte Carlo estimates one has to apply variance reduction techniques. In the present paper a procedure of source importance sampling is applied. This means that start locations of the source particles are sampled in such a way to increase a probability

2.4. Description of the variance reduction technique

for the source photon to hit the target region of interest. In other words, the source particles distribution is intentionally biased to increase scoring in the target regions. The bias in the source distribution is compensated by adjusting weights of the source photons. After the source particle is initiated, no other weight adjustment is made, thus preserving the analogue simulation of the radiation transport. Details of this technique, known as «importance sampling», can be found elsewhere (see e.g. [16, 17, 18, 19]). Source sampling technique specific to the present study is summarized below.

The Monte Carlo estimation of an organ average absorbed dose, D , results in calculating the integral [16]:

$$D = \int_{\Gamma} g(\vec{x}) f(\vec{x}) d\vec{x}, \quad (2.11)$$

where $\vec{x} \equiv (\vec{r}, \vec{\Omega}, E)$ is a point in a domain Γ of the problem phase-space, $f(\vec{x})$ is a probability density function, and $g(\vec{x})$ is a probabilistic estimate of the dose response for a given \vec{x} .

The source bias is described by means of importance function, $f^*(\vec{x})$, and introduced into the above equation in the following way:

$$D = \int_{\Gamma} g(\vec{x}) \frac{f(\vec{x})}{f^*(\vec{x})} f^*(\vec{x}) d\vec{x}. \quad (2.12)$$

Now, Eq. (2.12) is an integration over *biased* distribution, $f^*(\vec{x})$, and contributions to the integral, $g(\vec{x})$, are made with weights

$$w = \frac{f(\vec{x})}{f^*(\vec{x})}. \quad (2.13)$$

Selection of an appropriate importance function is a rather delicate issue. In Monte Carlo literature (see references above) it was shown that the use of the importance function

$$f^*(\vec{x}) = \frac{g(\vec{x}) f(\vec{x})}{D} \quad (2.14)$$

leads to a zero-variance Monte Carlo estimate. Although, this recipe is useless practically (with knowledge of the answer, D , no one needs to solve Eqn.

2. Materials and Methods

(2.11)), nevertheless it gives a criterion for an appropriate selection of the importance function, $f^*(\vec{x})$.

Let us consider Eqn. (2.14) in details. In the present work the problem phase-space is limited to spatial co-ordinates, only. This is because the photon sources being considered have pre-defined set of energies and directions³. Then, $\vec{x} \equiv \vec{r}$ and the spatial co-ordinates are sampled from the uniform distribution, i.e. $f(\vec{r}) = \text{const.}$ The expected value of the dose, D , is a constant number, also. Therefore, the shape of the importance function (2.14) is determined by the function $g(\vec{r})$ and one has to estimate (at least, roughly and qualitatively) this function. The following reasoning is applied to justify a selection of an analytical form of the importance function.

The problem of Monte Carlo estimation of the tooth dose response to extended planar photon source⁴ can be roughly approximated by a problem of an infinite planar source and a point target. Then, one can apply the reciprocity principle (see e.g. Sec. 2.7 in [20]), namely, one can assume inverse geometry of point isotropic source and infinite planar target. It is known (see e.g. Hudson, 1964) that for such geometry a distribution of co-ordinates of particle hits into the target plane follows a resonance-shape Cauchy (Lorentzian) probability density distribution

$$f_c(\vec{r}) = \frac{\beta}{\pi ((\vec{r} - \vec{r}_0)^2 + \beta^2)}, \quad (2.15)$$

where \vec{r}_0 is a coordinate vector of a point on a target plane closest to the source point, β is equal numerically to the minimum distance between the source point and the target plane. The parameter β has explicit physical meaning as a half of a resonance full-width at half-maximum height. From the Eqn. (2.14) it follows that if $g(\vec{r}) \sim f_c(\vec{r})$ then the importance function has a shape of Cauchy distribution: $f^*(\vec{r}) \sim f_c(\vec{r})$. The main advantages of using the Cauchy distribution as an importance function are:

³Generally speaking, the importance sampling of the source can be done by directional biasing, also, but in this report this is not considered.

⁴An isotropic field can be modeled on a surface as a source with cosine angular distribution (see e.g. p. 19 in [18]).

2.4. Description of the variance reduction technique

- clear physical sense resulted from the reciprocity principle, and
- parameters of the distribution are pre-defined by the problem geometry.

The algorithm for sampling spatial co-ordinates is implemented in the following way. The source photons are sampled on planes orthogonal to co-ordinate axes. This results in sampling for every surface only two independent variables, say u and v . Because of variables independence the joint probability density function is $f_c(\vec{r}) = f_c(u)f_c(v)$, and the sampling is done independently for the both variables using the same procedure.

For any of two independent variables, say for u , the univariate Cauchy and the uniform, $f_{uni} = (u_{max} - u_{min})^{-1}$, probability density distributions are shown in Fig. 2.2. Both distributions are defined for $u \in [u_{min}, u_{max}]$.

The Cauchy probability density distribution must be normalized:

$$\tilde{f}_c(u) = \frac{f_c(u)}{F_c(u_{max}) - F_c(u_{min})} = \frac{f_c(u)}{\Delta F_c}, \quad (2.16)$$

where $F_c(u)$ is Cauchy probability distribution function:

$$F_c(u) = \int_{-\infty}^u f_c(u') du' = \frac{1}{2} + \frac{1}{\pi} \arctan\left(\frac{u - u_0}{\beta}\right).$$

Random sampling from the distribution function (2.16) gives a value of co-ordinate u_r and the source particle is assigned the following initial statistical weight:

$$w(u_r) = \frac{f_{uni}(u_r)}{\tilde{f}_c(u_r)} = \pi \left(1 + \left(\frac{u_r - u_0}{\beta}\right)^2\right) \frac{\Delta F_c}{u_{max} - u_{min}}. \quad (2.17)$$

The same procedure applied to the second variable gives a value of v_r and of corresponding statistical weight, $w(v_r)$. Thus, the total weight of the source particle started from the given plane surface is

$$w(u_r, v_r) = w(u_r)w(v_r). \quad (2.18)$$

Eqn. (2.18) is applicable to the case of sampling a source particle for the monodirectional exposure geometry on a given planar surface. To sample

2. Materials and Methods

source particles in ROT- and ISO-geometries one needs to sample first a surface, then the problem is reduced to the one considered above. The distribution to sample i^{th} surface is constructed in the following way:

$$w_i = \frac{\Delta F_c(u_i)\Delta F_c(v_i)}{\sum_s \Delta F_c(u_s)\Delta F_c(v_s)},$$

where $\Delta F_c(u) = F_c(u_{max}) - F_c(u_{min})$ and $s = 1, \dots, n$ ($n = 4$ for ROT- and $n = 6$ for ISO-geometry).

2.5. Scoring

Dose conversion coefficients for tooth cells, $C_{f,T}(E)$, have been estimated using Eqn. (2.1), namely as a ratio of the dose in a specific region and a value of the fluence of the given radiation source. The following analytical estimates have been taken for the total fluence normalized per source photon (in the ROT- and ISO-geometries only inward directed particles were sampled):

1. $\Phi_{PAR} = \frac{1}{A_S}$ for parallel beams, i.e. for AP, PA, LLAT, RLAT, TOP, and CC sources;
2. $\Phi_{ROT} = \frac{\pi}{2A_S}$ for the ROT-source;
3. $\Phi_{ISO} = \frac{2\pi}{A_S}$ for the ISO-source,

where A_S is an area of the source surface. For the quality assurance purposes the fluences were also assessed numerically in every run.

Conversion of the coefficients $C_{f,T}(E)$ (dose per unit fluence) to $C_{k,T}(E)$ (dose per unit kerma) has been achieved, according to Eqn. (2.6), with the free-in-air kerma per unit fluence values, $k_{tr}(E)$, taken from Table A.1 in [10].

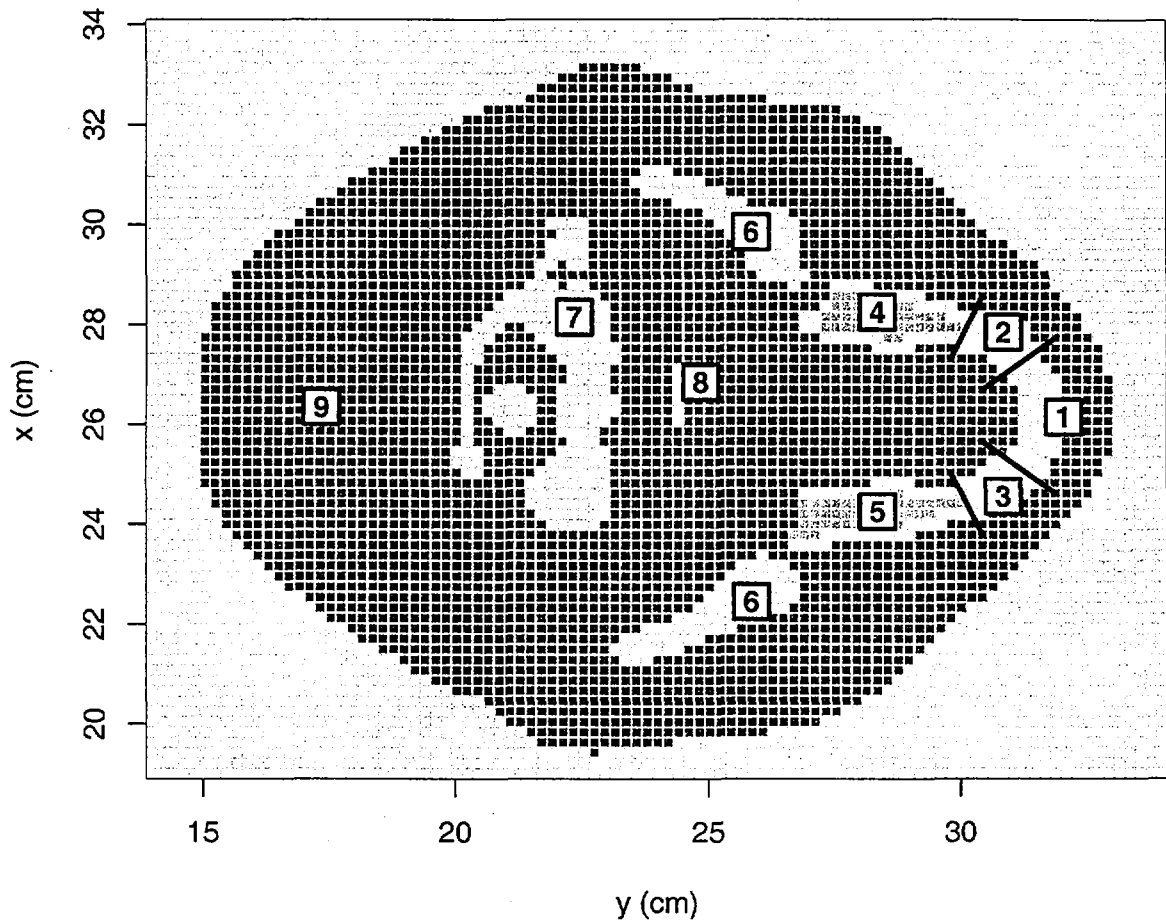


Figure 2.1.: Slice of the "Golem" phantom head showing tooth cells and their separation into five locations: (1) Front, (2) Front-Left, (3) Front-Right, (4) Left, and (5) Right. Also indicated are: (6) bone, (7) spine and spinal cord, (8) trachea, and (9) soft tissues.

2. Materials and Methods

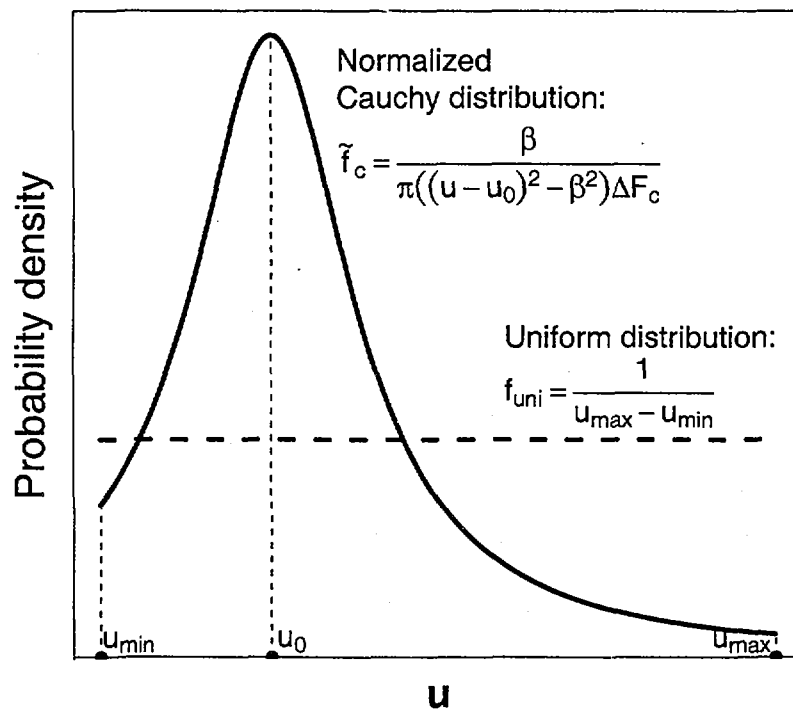


Figure 2.2.: Illustration of the source importance sampling for arbitrary spatial coordinate u . Shown are univariate normalized Cauchy (solid line) and uniform (dashed line) probability density distributions.

3. Results

3.1. Dose conversion coefficients for tooth enamel

The tooth DCCs are calculated for eight irradiation geometries, 18 monoenergetic photon sources, and 30 cells representing buccal/lingual enamel and dentine grouped into five locations in two slices (upper and lower jaws). Thus, the total number of energy-dependent dose responses is equal to 240, and, obviously, manual processing of these data is cumbersome. To automate handling of the calculated data a special-purpose software utility has been developed using the Python programming language¹. The utility operates on a database of the results from the present Monte Carlo simulations. The data are stored in separate files for each of the eight geometries considered. Each file contains for 30 tooth cells the following data:

- energy grid: 18 values in the energy range from 0.01 MeV to 10 MeV;
- computed values of absorbed dose per free-in-air kerma;
- absolute statistical error of the Monte Carlo estimate (2σ -values).

The utility performs two basic tasks. First, it eases a handling of the numerous DCCs computed in the present study by storing and plotting them. The coefficients can be plotted for different geometries and target cells. The dose responses for different target cells can be plotted separately or they can be combined together, i.e. a user can plot and investigate the dose coefficients separately for every material and location or can plot averaged dose coefficients for certain materials and/or locations.

¹www.python.org

3. Results

Secondly, the utility allows a user to input energy-dependent continuous or discrete photon fluence and to compute integral tooth dose and air-kerma according to Eqns. (2.8) and (2.9) by numerical integration over the user-defined fluence. A possibility exists for integration over the user-defined fluence of equivalent or effective doses (Eqn. (2.10)) using data from ICRP Publication 74 [7], which are also included in the database of the dose conversion coefficients. The conversion factors defined in Eqn. (4.1) and (4.2) are also computed. These allow converting measured absorbed dose in tooth enamel to integral air kerma and integral organ dose for the given energy-dependent fluence. More details on the utility, including screenshots, can be found in Appendix.

Presented in Tables 3.1 – 3.8 are numerical values of the dose conversion coefficients for buccal and lingual enamel in eight simulated irradiation geometries. Given in brackets are values of the coefficient of variation (CV) in percent. The data in the tables are presented for all five locations (segments) in RLAT and LLAT geometries. In other irradiation geometries, due to symmetry of the phantom and of the irradiation geometry the dose responses are averaged between left and right segments. Also, to reduce the table sizes the data in the Tables 3.1–3.8 are given as mass-weighted averages for the upper and lower jaws. Such averaging appears to be an adequate procedure for the AP, PA, LLAT, RLAT, ROT, and ISO geometries as the data for both jaws are very similar. However, there ought to be differences in dose responses for the TOP and CC geometries because of a shielding of one jaw by another when the source photons are directed parallel to the z -axis. The enamel dose responses averaged over all segments and enamel layers are given in Fig. 3.1 for the TOP and CC geometries and for different jaws, separately. It can be seen from the figure that noticeable differences between dose responses for the upper and lower jaws (more than 10%) are present for the TOP geometry in the energy range from 40 keV to 300 keV and the maximum difference (up to 30%) is observed at energy 50 keV. In the CC geometry the differences in DCCs for different jaws are negligible.

From the Tables 3.1 – 3.8 one can see that the dose conversion coefficients demonstrate strong non-linear energy dependence at photon energies below

3.1. Dose conversion coefficients for tooth enamel

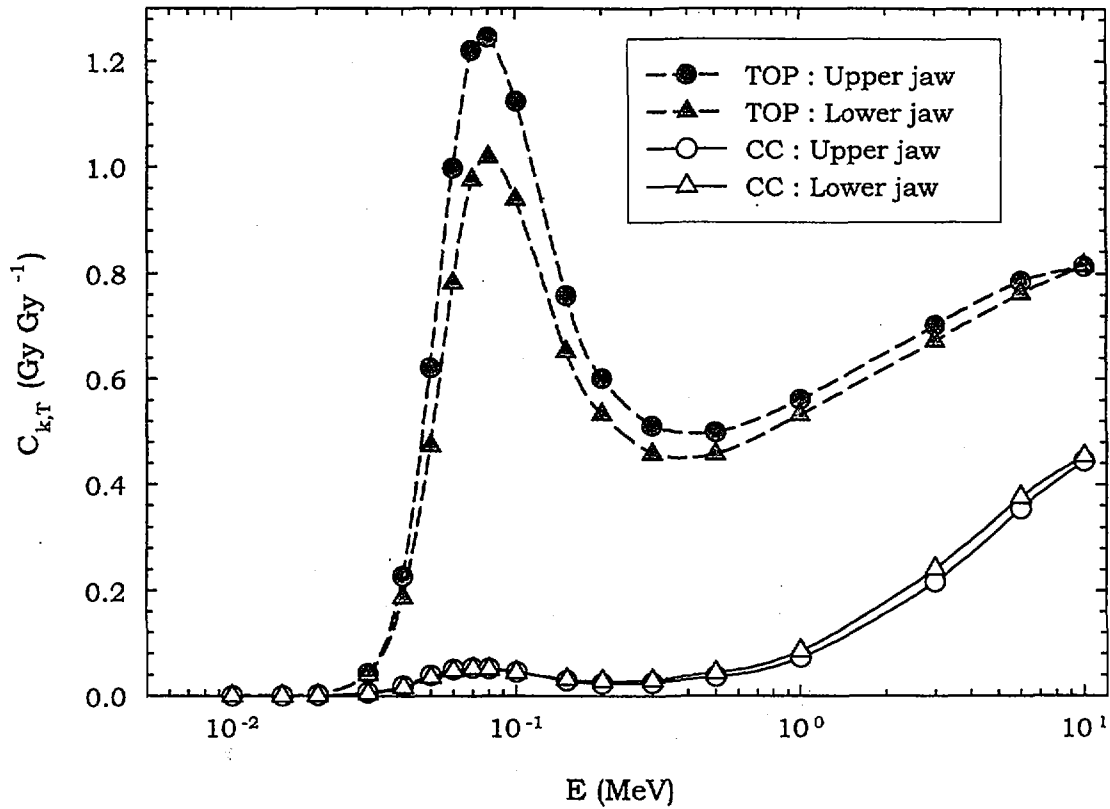


Figure 3.1.: Dose conversion coefficients for tooth enamel in the upper and lower jaws. The coefficients are averaged over locations and buccal/lingual layers. Closed symbols – TOP source; open symbols – CC source.

300 keV. Maxima of the energy-dependence are observed at energies between 50 and 90 keV. For monodirectional sources, the energy dependence in that energy range varies considerably between different locations. For the photon sources with cylindrical (ROT) and spherical (ISO) symmetry, variations of the dose conversion coefficients between different locations are less and more important for buccal enamel. This fact is quite remarkable as these geometries (ROT and ISO) are of special interest for the occupational dose reconstruction problems.

3. Results

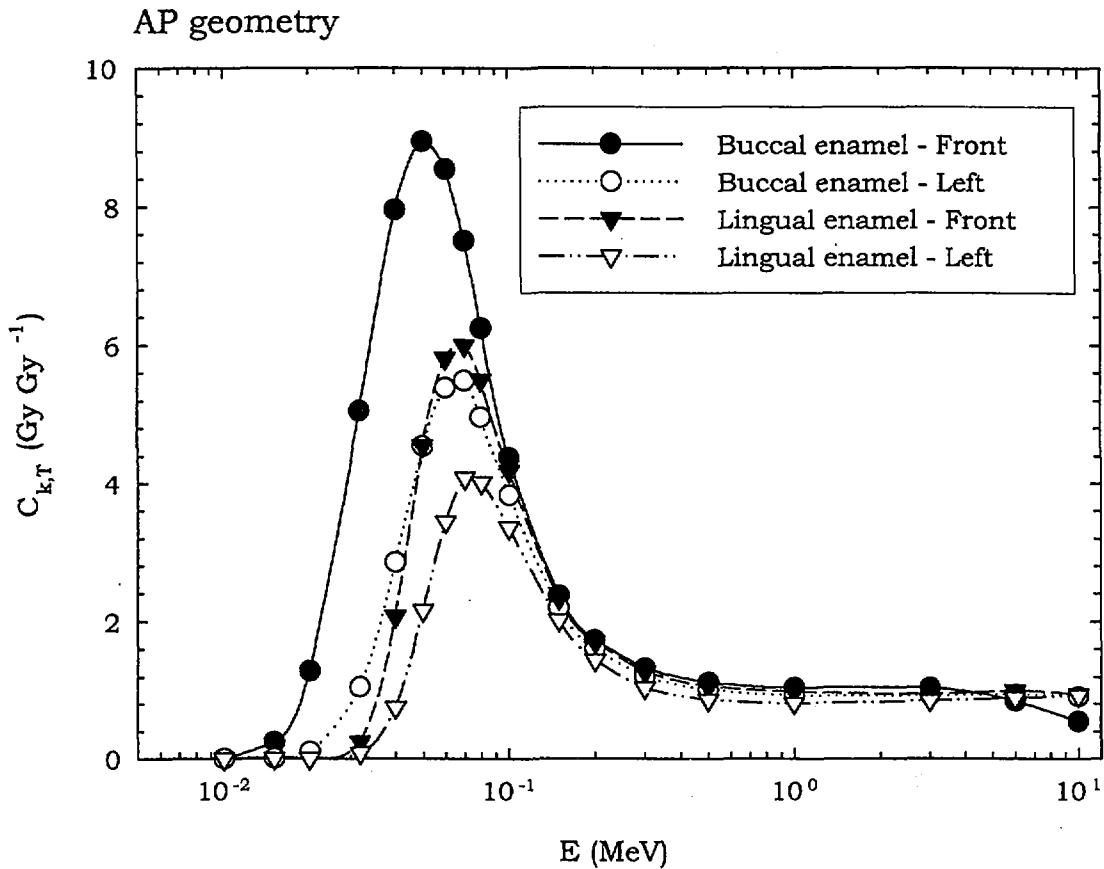


Figure 3.2.: Tooth enamel dose conversion coefficients for different locations/layers in AP irradiation geometry. The coefficients are averaged over upper and lower jaws. Closed symbols — location «Front»; open symbols — location «Left».

Examples of the energy dependence of the dose conversion coefficients for AP and ROT irradiation geometries are given in Figs. 3.2 and 3.3. From these, one can readily conclude that the relationship between integral enamel dose, (Eqn. (2.9)), and integral air kerma, (Eqn. (2.8)), or integral organ dose, (Eqn. (2.10)), is non-linear and is determined by energy dependence of a photon fluence and DCCs, (more on this issue see in Section 4).

3.2. Simulation of coupled electron-photon transport

As already mentioned, the dose conversion coefficients presented in this report are computed by taking into account coupled photon-electron transport. Several different values of electron cut-off energy were investigated and a cut-off value equal to 100 keV was selected for the calculations. Such a relatively high cut-off value is sufficient for the simulation as the target regions – tooth cells – are isolated from the body-air interface by soft tissue. That is, a reduction of the enamel dose due to electron escape from a tooth cell is compensated by secondary electrons coming from the surrounding soft tissues and dentine. Because of differences in the densities of teeth and soft tissues, this situation is unlikely to be the case of electron equilibrium. Nonetheless, an effect of the electron leakage from the enamel cells is not seen for energies less than approximately 3 MeV. Only at energies higher than 3 MeV, where the electron range in soft tissue becomes comparable with the thickness of overlaying soft tissues, the leakage of electrons from the phantom through the body-air interface becomes noticeable and results in reduction of absorbed dose in the tooth enamel. This is illustrated by the data in Table 3.9, where the ratios of the dose conversion coefficients computed without electron transport (kerma approximation) and with electron transport are presented. The ratios are given for buccal/lingual enamel and dentine in the «Front» location for the AP geometry. As it can be seen from the Table 3.9, under the given conditions the electron transport can be safely ignored for incident photon energies for up to at least 3 MeV.

3. Results

Table 3.1.: Jaw-averaged enamel DCCs, $C_{k,T}$, for the AP-geometry at different locations. Shown in the brackets are values of the coefficient of variation (CV).

E (MeV)	Dose conversion coefficient $C_{k,T}$ (Gy Gy ⁻¹) [CV (%)]		
	Front	Front-Left and Front-Right	Left and Right
Buccal enamel			
0.01	3.5×10^{-3} [0.1]	1.3×10^{-3} [0.2]	2.6×10^{-6} [3.3]
0.015	2.5×10^{-1} [0.0]	1.1×10^{-1} [0.1]	7.0×10^{-3} [0.7]
0.02	1.3 [0.0]	6.5×10^{-1} [0.1]	1.2×10^{-1} [0.3]
0.03	5.1 [0.1]	3.3 [0.2]	1.1 [0.3]
0.04	8.0 [0.2]	6.2 [0.3]	3.0 [0.4]
0.05	8.9 [0.3]	7.7 [0.5]	4.7 [0.5]
0.06	8.5 [0.4]	7.8 [0.6]	5.5 [0.6]
0.07	7.5 [0.6]	7.1 [0.8]	5.6 [0.7]
0.08	6.3 [0.7]	6.1 [1.1]	5.0 [0.8]
0.1	4.4 [1.0]	4.3 [1.2]	3.9 [0.9]
0.15	2.4 [1.3]	2.4 [1.6]	2.2 [1.3]
0.2	1.7 [1.1]	1.7 [1.4]	1.6 [1.3]
0.3	1.3 [1.0]	1.3 [1.2]	1.2 [1.0]
0.5	1.1 [0.8]	1.1 [0.9]	1.0 [0.8]
1.0	1.0 [0.8]	1.0 [1.1]	9.3×10^{-1} [0.8]
3.0	1.0 [0.9]	1.0 [1.1]	9.2×10^{-1} [0.9]
6.0	8.4×10^{-1} [0.9]	9.0×10^{-1} [1.2]	9.4×10^{-1} [0.9]
10.0	5.5×10^{-1} [1.0]	6.9×10^{-1} [1.3]	9.1×10^{-1} [0.9]
Lingual enamel			
0.01	—	—	—
0.015	1.5×10^{-5} [36.2]	1.3×10^{-5} [44.2]	1.3×10^{-6} [38.2]
0.02	9.0×10^{-4} [3.5]	7.6×10^{-4} [4.8]	3.6×10^{-4} [18.5]
0.03	2.4×10^{-1} [0.7]	1.3×10^{-1} [1.3]	7.7×10^{-2} [3.0]
0.04	2.1 [0.5]	1.4 [0.9]	7.5×10^{-1} [1.2]
0.05	4.6 [0.7]	3.6 [0.8]	2.2 [0.9]
0.06	5.8 [0.7]	5.1 [1.0]	3.4 [1.0]
0.07	6.0 [0.8]	5.5 [1.1]	4.1 [0.9]
0.08	5.5 [1.1]	5.1 [1.3]	4.0 [1.1]
0.1	4.2 [1.3]	4.0 [1.9]	3.4 [1.1]
0.15	2.3 [1.5]	2.3 [2.0]	2.0 [1.4]
0.2	1.7 [1.6]	1.6 [1.7]	1.4 [1.4]
0.3	1.3 [1.4]	1.2 [1.5]	1.0 [1.1]
0.5	1.1 [1.0]	1.0 [1.4]	8.7×10^{-1} [1.0]
1.0	9.8×10^{-1} [1.0]	9.5×10^{-1} [1.3]	8.1×10^{-1} [0.9]
3.0	9.5×10^{-1} [1.1]	9.4×10^{-1} [1.5]	8.5×10^{-1} [1.0]
6.0	1.0 [1.0]	9.8×10^{-1} [1.4]	8.9×10^{-1} [0.9]
10.0	9.4×10^{-1} [0.9]	9.8×10^{-1} [1.2]	9.3×10^{-1} [0.9]

3.2. Simulation of coupled electron-photon transport

Table 3.2.: Jaw-averaged enamel DCCs, $C_{k,T}$, for the PA-geometry at different locations. Shown in the brackets are values of the coefficient of variation (CV).

E (MeV)	Dose conversion coefficient $C_{k,T}$ (Gy Gy ⁻¹) [CV (%)]		
	Front	Front-Left and Front-Right	Left and Right
Buccal enamel			
0.01	—	—	—
0.015	—	—	—
0.02	—	7.3×10^{-5} [31.6]	1.7×10^{-4} [22.0]
0.03	1.0×10^{-3} [32.4]	4.7×10^{-3} [11.0]	2.7×10^{-2} [2.3]
0.04	3.2×10^{-2} [5.9]	5.0×10^{-2} [7.0]	2.2×10^{-1} [1.6]
0.05	1.6×10^{-1} [4.4]	1.8×10^{-1} [5.0]	6.6×10^{-1} [1.6]
0.06	3.4×10^{-1} [3.6]	3.9×10^{-1} [4.2]	1.1 [1.6]
0.07	5.1×10^{-1} [3.4]	5.4×10^{-1} [4.0]	1.4 [1.7]
0.08	5.8×10^{-1} [3.5]	6.2×10^{-1} [3.9]	1.4 [1.8]
0.1	5.8×10^{-1} [3.6]	6.5×10^{-1} [4.1]	1.3 [2.0]
0.15	4.5×10^{-1} [3.5]	4.9×10^{-1} [4.1]	8.9×10^{-1} [2.1]
0.2	3.8×10^{-1} [3.1]	4.2×10^{-1} [3.7]	7.0×10^{-1} [2.0]
0.3	3.5×10^{-1} [2.8]	3.6×10^{-1} [3.3]	5.8×10^{-1} [1.8]
0.5	3.9×10^{-1} [2.4]	3.6×10^{-1} [3.1]	5.5×10^{-1} [1.9]
1.0	4.7×10^{-1} [2.5]	4.3×10^{-1} [3.3]	5.9×10^{-1} [2.1]
3.0	6.2×10^{-1} [2.5]	5.7×10^{-1} [3.3]	7.0×10^{-1} [2.2]
6.0	7.3×10^{-1} [2.1]	6.9×10^{-1} [3.0]	7.9×10^{-1} [2.1]
10.0	7.9×10^{-1} [1.8]	7.4×10^{-1} [2.6]	8.2×10^{-1} [2.0]
Lingual enamel			
0.01	—	—	—
0.015	—	—	—
0.02	—	—	3.5×10^{-5} [41.8]
0.03	6.4×10^{-3} [3.2]	4.5×10^{-3} [6.1]	1.5×10^{-2} [2.8]
0.04	1.3×10^{-1} [3.6]	1.1×10^{-1} [4.1]	2.0×10^{-1} [1.7]
0.05	4.1×10^{-1} [2.5]	3.9×10^{-1} [3.2]	6.7×10^{-1} [1.5]
0.06	6.9×10^{-1} [2.8]	6.9×10^{-1} [3.4]	1.1 [1.6]
0.07	8.8×10^{-1} [2.9]	9.0×10^{-1} [3.7]	1.5 [1.6]
0.08	9.4×10^{-1} [3.0]	9.5×10^{-1} [3.9]	1.5 [1.8]
0.1	8.9×10^{-1} [3.3]	9.3×10^{-1} [4.0]	1.4 [1.9]
0.15	6.5×10^{-1} [3.6]	6.7×10^{-1} [3.9]	9.4×10^{-1} [2.0]
0.2	5.2×10^{-1} [3.2]	5.5×10^{-1} [3.8]	7.4×10^{-1} [2.0]
0.3	4.5×10^{-1} [2.8]	4.7×10^{-1} [3.6]	6.0×10^{-1} [1.9]
0.5	4.7×10^{-1} [2.7]	4.7×10^{-1} [3.4]	5.5×10^{-1} [1.9]
1.0	5.4×10^{-1} [2.9]	5.3×10^{-1} [3.6]	5.8×10^{-1} [2.2]
3.0	7.2×10^{-1} [2.9]	6.8×10^{-1} [3.8]	6.9×10^{-1} [2.4]
6.0	8.1×10^{-1} [2.5]	7.5×10^{-1} [3.5]	7.8×10^{-1} [2.3]
10.0	8.3×10^{-1} [2.1]	8.1×10^{-1} [3.0]	8.2×10^{-1} [2.1]

3. Results

Table 3.3.: Jaw-averaged enamel DCCs, $C_{k,T}$, for the LLAT-geometry at different locations. Shown in the brackets are values of the coefficient of variation (CV).

E (MeV)	Dose conversion coefficient $C_{k,T}$ (Gy Gy ⁻¹) [CV (%)]				
	Front	Front-Left	Front-Right	Left	Right
Buccal enamel					
0.01	2.5×10^{-4} [0.8]	9.8×10^{-4} [0.2]	—	7.4×10^{-6} [0.4]	—
0.015	3.8×10^{-2} [0.1]	1.3×10^{-1} [0.1]	1.1×10^{-4} [1.0]	2.6×10^{-2} [0.1]	5.0×10^{-6} [1.0]
0.02	2.6×10^{-1} [0.1]	8.7×10^{-1} [0.1]	3.8×10^{-3} [1.3]	4.1×10^{-1} [0.1]	5.5×10^{-5} [3.0]
0.03	1.4 [0.2]	4.1 [0.2]	6.6×10^{-2} [1.2]	3.1 [0.1]	1.8×10^{-2} [2.1]
0.04	3.1 [0.4]	7.2 [0.3]	3.1×10^{-1} [1.4]	5.9 [0.2]	2.7×10^{-1} [1.1]
0.05	4.5 [0.5]	8.4 [0.5]	9.6×10^{-1} [1.3]	7.4 [0.4]	1.0 [1.0]
0.06	5.0 [0.7]	8.0 [0.7]	1.7 [1.4]	7.6 [0.5]	1.8 [1.0]
0.07	4.8 [0.9]	7.3 [0.9]	2.1 [1.5]	7.1 [0.6]	2.3 [1.1]
0.08	4.3 [1.0]	6.0 [1.0]	2.2 [1.6]	6.1 [0.7]	2.4 [1.1]
0.1	3.2 [1.2]	4.3 [1.3]	1.9 [1.8]	4.4 [0.8]	2.1 [1.2]
0.15	1.8 [1.3]	2.3 [1.4]	1.3 [1.9]	2.5 [0.9]	1.4 [1.4]
0.2	1.4 [1.2]	1.7 [1.4]	1.0 [1.7]	1.8 [0.9]	1.1 [1.3]
0.3	1.1 [1.2]	1.3 [1.4]	8.4×10^{-1} [1.7]	1.3 [0.9]	8.3×10^{-1} [1.3]
0.5	1.0 [1.3]	1.2 [1.5]	7.7×10^{-1} [1.8]	1.1 [1.1]	7.5×10^{-1} [1.4]
1.0	9.5×10^{-1} [1.6]	1.0 [1.9]	7.8×10^{-1} [2.1]	1.0 [1.3]	7.3×10^{-1} [1.7]
3.0	9.4×10^{-1} [1.9]	1.0 [2.1]	8.2×10^{-1} [2.4]	1.0 [1.5]	8.1×10^{-1} [1.8]
6.0	9.1×10^{-1} [1.9]	9.4×10^{-1} [2.1]	8.8×10^{-1} [2.1]	1.0 [1.4]	8.7×10^{-1} [1.6]
10.0	8.4×10^{-1} [1.9]	6.8×10^{-1} [2.2]	9.4×10^{-1} [1.8]	9.0×10^{-1} [1.2]	9.2×10^{-1} [1.3]
Lingual enamel					
0.01	—	—	—	—	—
0.015	2.2×10^{-5} [36.1]	2.0×10^{-5} [36.1]	—	4.9×10^{-6} [1.0]	—
0.02	5.9×10^{-4} [1.4]	1.4×10^{-3} [3.0]	5.3×10^{-5} [6.3]	6.4×10^{-4} [2.9]	3.4×10^{-4} [2.8]
0.03	7.1×10^{-2} [1.2]	1.9×10^{-1} [0.9]	5.1×10^{-2} [1.8]	1.6×10^{-1} [0.6]	9.0×10^{-2} [0.8]
0.04	8.0×10^{-1} [0.8]	1.8 [0.7]	6.9×10^{-1} [1.1]	1.5 [0.5]	8.2×10^{-1} [0.7]
0.05	2.3 [0.9]	3.9 [0.9]	2.0 [1.2]	3.6 [0.5]	2.1 [0.7]
0.06	3.5 [1.0]	5.2 [1.0]	3.0 [1.3]	4.8 [0.6]	3.1 [0.8]
0.07	4.0 [1.1]	5.5 [1.2]	3.5 [1.5]	5.3 [0.7]	3.6 [0.9]
0.08	3.9 [1.2]	4.9 [1.3]	3.3 [1.7]	4.9 [0.8]	3.4 [1.0]
0.1	3.1 [1.4]	3.8 [1.5]	2.7 [1.9]	3.9 [0.9]	2.9 [1.1]
0.15	1.9 [1.5]	2.2 [1.7]	1.7 [2.0]	2.3 [1.0]	1.7 [1.2]
0.2	1.4 [1.5]	1.6 [1.7]	1.3 [2.0]	1.6 [1.0]	1.3 [1.2]
0.3	1.1 [1.5]	1.3 [1.7]	1.0 [1.9]	1.2 [1.0]	9.8×10^{-1} [1.2]
0.5	9.5×10^{-1} [1.7]	1.1 [1.9]	9.0×10^{-1} [2.1]	1.0 [1.2]	8.5×10^{-1} [1.4]
1.0	8.9×10^{-1} [2.0]	9.7×10^{-1} [2.3]	8.9×10^{-1} [2.5]	9.3×10^{-1} [1.5]	8.2×10^{-1} [1.6]
3.0	9.2×10^{-1} [2.3]	9.8×10^{-1} [2.7]	9.1×10^{-1} [2.8]	9.2×10^{-1} [1.7]	8.9×10^{-1} [1.8]
6.0	9.4×10^{-1} [2.3]	1.0 [2.4]	9.5×10^{-1} [2.6]	9.7×10^{-1} [1.5]	9.3×10^{-1} [1.6]
10.0	9.7×10^{-1} [2.1]	9.8×10^{-1} [2.1]	9.6×10^{-1} [2.2]	1.0 [1.2]	9.1×10^{-1} [1.3]

3.2. Simulation of coupled electron-photon transport

Table 3.4.: Jaw-averaged enamel DCCs, $C_{k,T}$, for the RLAT-geometry at different locations. Shown in the brackets are values of the coefficient of variation (CV).

E (MeV)	Dose conversion coefficient $C_{k,T}$ (Gy Gy ⁻¹) [CV (%)]				
	Front	Front-Left	Front-Right	Left	Right
Buccal enamel					
0.01	8.8×10^{-5} [0.1]	—	8.0×10^{-4} [0.1]	—	1.2×10^{-5} [0.1]
0.015	2.5×10^{-2} [0.2]	1.1×10^{-4} [0.8]	1.3×10^{-1} [0.1]	2.3×10^{-6} [36.1]	2.9×10^{-2} [0.1]
0.02	2.1×10^{-1} [0.1]	3.5×10^{-3} [1.1]	8.1×10^{-1} [0.1]	5.1×10^{-5} [4.5]	4.5×10^{-1} [0.1]
0.03	1.4 [0.2]	6.6×10^{-2} [1.2]	3.9 [0.2]	1.7×10^{-2} [1.6]	3.2 [0.1]
0.04	3.0 [0.4]	3.3×10^{-1} [1.3]	6.8 [0.3]	2.6×10^{-1} [1.1]	6.1 [0.2]
0.05	4.4 [0.6]	9.8×10^{-1} [1.4]	8.2 [0.5]	9.8×10^{-1} [0.9]	7.5 [0.4]
0.06	4.9 [0.7]	1.7 [1.4]	8.0 [0.7]	1.8 [1.0]	7.6 [0.5]
0.07	4.8 [0.9]	2.2 [1.5]	7.2 [0.9]	2.3 [1.0]	7.1 [0.7]
0.08	4.1 [1.0]	2.2 [1.7]	6.0 [1.0]	2.3 [1.1]	6.1 [0.8]
0.1	3.2 [1.2]	2.0 [1.8]	4.2 [1.3]	2.1 [1.2]	4.5 [0.9]
0.15	1.8 [1.3]	1.3 [1.9]	2.3 [1.4]	1.3 [1.3]	2.4 [1.0]
0.2	1.4 [1.3]	1.0 [1.8]	1.7 [1.4]	1.0 [1.3]	1.8 [1.0]
0.3	1.1 [1.2]	8.2×10^{-1} [1.8]	1.3 [1.4]	8.2×10^{-1} [1.2]	1.3 [1.0]
0.5	9.9×10^{-1} [1.4]	7.7×10^{-1} [1.9]	1.1 [1.5]	7.4×10^{-1} [1.3]	1.1 [1.2]
1.0	9.3×10^{-1} [1.6]	7.7×10^{-1} [2.2]	1.0 [1.9]	7.4×10^{-1} [1.6]	1.0 [1.5]
3.0	9.5×10^{-1} [1.9]	8.3×10^{-1} [2.5]	1.0 [2.1]	8.0×10^{-1} [1.8]	1.0 [1.6]
6.0	9.3×10^{-1} [1.9]	8.7×10^{-1} [2.3]	9.4×10^{-1} [2.1]	8.7×10^{-1} [1.5]	1.0 [1.4]
10.0	8.6×10^{-1} [1.9]	9.1×10^{-1} [1.9]	6.8×10^{-1} [2.3]	9.2×10^{-1} [1.3]	8.9×10^{-1} [1.3]
Lingual enamel					
0.01	—	—	—	—	—
0.015	—	—	—	—	—
0.02	1.2×10^{-4} [2.2]	1.1×10^{-4} [10.2]	4.3×10^{-4} [19.0]	3.0×10^{-4} [5.4]	8.3×10^{-4} [3.3]
0.03	6.0×10^{-2} [1.1]	4.9×10^{-2} [1.6]	2.2×10^{-1} [0.9]	8.6×10^{-2} [0.8]	1.6×10^{-1} [0.6]
0.04	7.8×10^{-1} [0.9]	7.0×10^{-1} [1.1]	1.8 [0.8]	7.8×10^{-1} [0.7]	1.4 [0.5]
0.05	2.3 [0.9]	2.0 [1.2]	4.1 [0.9]	2.1 [0.7]	3.5 [0.6]
0.06	3.5 [1.0]	3.1 [1.3]	5.3 [1.0]	3.1 [0.8]	4.8 [0.7]
0.07	4.0 [1.1]	3.5 [1.5]	5.5 [1.2]	3.5 [0.9]	5.2 [0.7]
0.08	3.8 [1.2]	3.3 [1.6]	5.0 [1.4]	3.4 [0.9]	4.9 [0.8]
0.1	3.1 [1.4]	2.8 [1.8]	3.8 [1.6]	2.8 [1.1]	3.8 [1.0]
0.15	1.9 [1.6]	1.7 [2.0]	2.2 [1.8]	1.7 [1.2]	2.2 [1.1]
0.2	1.4 [1.5]	1.3 [1.9]	1.6 [1.8]	1.3 [1.2]	1.6 [1.1]
0.3	1.1 [1.5]	1.0 [1.9]	1.3 [1.7]	9.7×10^{-1} [1.2]	1.2 [1.1]
0.5	9.4×10^{-1} [1.7]	9.1×10^{-1} [2.1]	1.1 [2.0]	8.5×10^{-1} [1.3]	1.0 [1.3]
1.0	9.0×10^{-1} [2.0]	8.7×10^{-1} [2.5]	9.8×10^{-1} [2.5]	8.2×10^{-1} [1.6]	9.3×10^{-1} [1.6]
3.0	9.0×10^{-1} [2.4]	9.4×10^{-1} [2.8]	9.7×10^{-1} [2.9]	8.9×10^{-1} [1.7]	9.3×10^{-1} [1.8]
6.0	9.5×10^{-1} [2.3]	9.6×10^{-1} [2.5]	1.0 [2.6]	9.3×10^{-1} [1.6]	9.6×10^{-1} [1.6]
10.0	9.6×10^{-1} [2.1]	9.7×10^{-1} [2.1]	1.0 [2.2]	9.1×10^{-1} [1.3]	1.0 [1.3]

3. Results

Table 3.5.: Jaw-averaged enamel DCCs, $C_{k,T}$, for the TOP-geometry at different locations. Shown in the brackets are values of the coefficient of variation (CV).

E (MeV)	Dose conversion coefficient $C_{k,T}$ (Gy Gy ⁻¹) [CV (%)]		
	Front	Front-Left and Front-Right	Left and Right
Buccal enamel			
0.01	—	—	—
0.015	3.2×10^{-4} [1.8]	2.2×10^{-4} [7.8]	5.1×10^{-6} [35.2]
0.02	1.1×10^{-2} [0.5]	5.4×10^{-3} [2.2]	5.7×10^{-4} [8.0]
0.03	1.8×10^{-1} [0.5]	8.3×10^{-2} [1.3]	2.1×10^{-2} [2.7]
0.04	5.8×10^{-1} [0.7]	3.1×10^{-1} [1.2]	1.7×10^{-1} [1.5]
0.05	1.0 [0.9]	6.8×10^{-1} [1.4]	5.2×10^{-1} [1.2]
0.06	1.3 [1.1]	9.9×10^{-1} [1.5]	8.9×10^{-1} [1.2]
0.07	1.4 [1.2]	1.1 [1.7]	1.1 [1.2]
0.08	1.3 [1.4]	1.2 [1.8]	1.2 [1.3]
0.1	1.1 [1.6]	1.0 [2.0]	1.1 [1.4]
0.15	7.3×10^{-1} [1.6]	6.8×10^{-1} [2.0]	7.4×10^{-1} [1.4]
0.2	5.9×10^{-1} [1.5]	5.5×10^{-1} [1.9]	5.9×10^{-1} [1.3]
0.3	5.3×10^{-1} [1.3]	4.9×10^{-1} [1.7]	5.0×10^{-1} [1.2]
0.5	5.4×10^{-1} [1.4]	5.0×10^{-1} [1.7]	4.9×10^{-1} [1.3]
1.0	6.1×10^{-1} [1.5]	5.7×10^{-1} [1.9]	5.6×10^{-1} [1.4]
3.0	7.5×10^{-1} [1.6]	7.1×10^{-1} [2.0]	6.9×10^{-1} [1.5]
6.0	8.1×10^{-1} [1.5]	7.9×10^{-1} [1.9]	7.7×10^{-1} [1.4]
10.0	8.5×10^{-1} [1.3]	8.0×10^{-1} [1.7]	8.1×10^{-1} [1.2]
Lingual enamel			
0.01	—	—	—
0.015	—	—	—
0.02	—	4.9×10^{-6} [44.2]	1.7×10^{-5} [9.1]
0.03	6.3×10^{-3} [4.1]	4.1×10^{-3} [8.2]	7.2×10^{-3} [3.8]
0.04	9.8×10^{-2} [2.0]	8.1×10^{-2} [3.0]	1.3×10^{-1} [1.5]
0.05	3.7×10^{-1} [1.7]	3.3×10^{-1} [2.3]	4.9×10^{-1} [1.2]
0.06	7.0×10^{-1} [1.7]	6.4×10^{-1} [2.2]	9.0×10^{-1} [1.2]
0.07	9.1×10^{-1} [1.8]	8.7×10^{-1} [2.3]	1.2 [1.2]
0.08	9.6×10^{-1} [1.9]	9.4×10^{-1} [2.4]	1.2 [1.3]
0.1	9.1×10^{-1} [2.0]	9.0×10^{-1} [2.5]	1.1 [1.4]
0.15	6.4×10^{-1} [2.1]	6.3×10^{-1} [2.6]	7.8×10^{-1} [1.4]
0.2	5.3×10^{-1} [1.9]	5.1×10^{-1} [2.4]	6.1×10^{-1} [1.4]
0.3	4.4×10^{-1} [1.7]	4.3×10^{-1} [2.2]	5.1×10^{-1} [1.3]
0.5	4.4×10^{-1} [1.8]	4.2×10^{-1} [2.3]	4.9×10^{-1} [1.3]
1.0	5.1×10^{-1} [2.0]	4.9×10^{-1} [2.5]	5.5×10^{-1} [1.5]
3.0	6.6×10^{-1} [2.1]	6.4×10^{-1} [2.6]	6.9×10^{-1} [1.6]
6.0	7.6×10^{-1} [1.9]	7.4×10^{-1} [2.4]	7.7×10^{-1} [1.5]
10.0	8.2×10^{-1} [1.6]	8.0×10^{-1} [2.1]	8.2×10^{-1} [1.3]

3.2. Simulation of coupled electron-photon transport

Table 3.6.: Jaw-averaged enamel DCCs, $C_{k,T}$, for the CC-geometry at different locations. Shown in the brackets are values of the coefficient of variation (CV).

E (MeV)	Dose conversion coefficient $C_{k,T}$ (Gy Gy ⁻¹) [CV (%)]		
	Front	Front-Left and Front-Right	Left and Right
Buccal enamel			
0.01	—	—	—
0.015	2.1×10^{-4} [1.0]	2.9×10^{-5} [1.5]	1.3×10^{-6} [44.2]
0.02	3.3×10^{-3} [1.1]	6.1×10^{-4} [2.9]	9.7×10^{-6} [25.5]
0.03	3.2×10^{-2} [1.5]	8.7×10^{-3} [3.3]	8.8×10^{-4} [8.8]
0.04	8.5×10^{-2} [1.9]	2.8×10^{-2} [4.0]	4.6×10^{-3} [8.5]
0.05	1.3×10^{-1} [2.6]	5.3×10^{-2} [5.1]	1.1×10^{-2} [7.9]
0.06	1.6×10^{-1} [3.6]	6.6×10^{-2} [6.7]	1.6×10^{-2} [10.5]
0.07	1.5×10^{-1} [4.6]	6.5×10^{-2} [8.4]	2.0×10^{-2} [10.3]
0.08	1.3×10^{-1} [5.4]	6.5×10^{-2} [9.3]	2.3×10^{-2} [11.0]
0.1	1.1×10^{-1} [6.5]	5.5×10^{-2} [10.3]	2.2×10^{-2} [11.7]
0.15	6.9×10^{-2} [7.0]	3.5×10^{-2} [11.8]	1.6×10^{-2} [11.9]
0.2	6.2×10^{-2} [6.4]	3.0×10^{-2} [10.7]	1.3×10^{-2} [11.7]
0.3	6.9×10^{-2} [5.2]	3.3×10^{-2} [9.3]	1.2×10^{-2} [10.8]
0.5	1.0×10^{-1} [4.6]	5.2×10^{-2} [7.6]	1.7×10^{-2} [9.7]
1.0	1.7×10^{-1} [3.8]	1.0×10^{-1} [6.1]	3.5×10^{-2} [8.1]
3.0	3.9×10^{-1} [3.0]	2.9×10^{-1} [4.3]	1.4×10^{-1} [4.7]
6.0	5.3×10^{-1} [2.6]	4.4×10^{-1} [3.4]	2.6×10^{-1} [3.4]
10.0	5.9×10^{-1} [2.2]	5.0×10^{-1} [3.0]	3.4×10^{-1} [2.7]
Lingual enamel			
0.01	—	—	—
0.015	—	—	—
0.02	—	9.7×10^{-6} [44.2]	—
0.03	8.8×10^{-4} [13.8]	4.9×10^{-4} [10.7]	1.6×10^{-4} [6.9]
0.04	1.2×10^{-2} [6.1]	5.9×10^{-3} [12.5]	2.8×10^{-3} [10.6]
0.05	3.8×10^{-2} [6.0]	2.2×10^{-2} [9.6]	1.0×10^{-2} [8.8]
0.06	5.7×10^{-2} [7.5]	3.7×10^{-2} [11.2]	1.8×10^{-2} [9.1]
0.07	7.2×10^{-2} [7.9]	4.4×10^{-2} [12.7]	2.2×10^{-2} [10.2]
0.08	6.6×10^{-2} [8.9]	4.3×10^{-2} [13.5]	2.6×10^{-2} [10.2]
0.1	6.1×10^{-2} [10.0]	4.2×10^{-2} [14.7]	2.2×10^{-2} [12.1]
0.15	4.5×10^{-2} [10.5]	2.7×10^{-2} [16.4]	1.6×10^{-2} [12.0]
0.2	3.6×10^{-2} [10.1]	2.4×10^{-2} [14.5]	1.4×10^{-2} [12.0]
0.3	3.7×10^{-2} [8.8]	2.6×10^{-2} [12.6]	1.2×10^{-2} [10.8]
0.5	5.7×10^{-2} [7.9]	4.0×10^{-2} [11.1]	1.5×10^{-2} [10.4]
1.0	1.2×10^{-1} [5.9]	8.4×10^{-2} [8.8]	3.1×10^{-2} [9.0]
3.0	3.0×10^{-1} [4.2]	2.5×10^{-1} [5.9]	1.3×10^{-1} [5.2]
6.0	4.6×10^{-1} [3.4]	4.0×10^{-1} [4.5]	2.4×10^{-1} [3.7]
10.0	5.6×10^{-1} [2.8]	5.0×10^{-1} [3.6]	3.3×10^{-1} [2.9]

3. Results

Table 3.7.: Jaw-averaged enamel DCCs, $C_{k,T}$, for the ROT-geometry at different locations. Shown in the brackets are values of the coefficient of variation (CV).

E (MeV)	Dose conversion coefficient $C_{k,T}$ (Gy Gy ⁻¹) [CV (%)]		
	Front	Front-Left and Front-Right	Left and Right
Buccal enamel			
0.01	1.0×10^{-3} [2.7]	8.4×10^{-4} [6.6]	9.6×10^{-6} [34.4]
0.015	8.0×10^{-2} [0.8]	6.2×10^{-2} [1.7]	1.1×10^{-2} [3.3]
0.02	4.4×10^{-1} [0.6]	3.6×10^{-1} [1.2]	1.4×10^{-1} [1.6]
0.03	2.0 [0.6]	1.7 [1.1]	1.1 [1.2]
0.04	3.6 [0.8]	3.2 [1.3]	2.3 [1.3]
0.05	4.4 [1.0]	4.1 [1.6]	3.4 [1.4]
0.06	4.5 [1.3]	4.3 [1.8]	3.9 [1.5]
0.07	4.3 [1.5]	4.2 [2.1]	4.0 [1.6]
0.08	3.7 [1.7]	3.7 [2.2]	3.7 [1.8]
0.1	2.7 [2.1]	2.8 [2.6]	2.9 [1.9]
0.15	1.6 [2.3]	1.6 [2.9]	1.7 [2.1]
0.2	1.2 [2.3]	1.2 [2.7]	1.3 [2.1]
0.3	9.6×10^{-1} [2.4]	9.6×10^{-1} [2.9]	9.9×10^{-1} [2.2]
0.5	8.6×10^{-1} [2.4]	8.5×10^{-1} [3.0]	8.5×10^{-1} [2.3]
1.0	8.3×10^{-1} [2.8]	8.4×10^{-1} [3.4]	8.1×10^{-1} [2.6]
3.0	8.8×10^{-1} [3.1]	8.9×10^{-1} [3.8]	8.7×10^{-1} [2.9]
6.0	8.4×10^{-1} [3.1]	8.6×10^{-1} [3.7]	9.1×10^{-1} [2.6]
10.0	7.6×10^{-1} [3.2]	7.8×10^{-1} [3.6]	8.9×10^{-1} [2.3]
Lingual enamel			
0.01	—	—	—
0.015	6.4×10^{-6} [37.3]	2.7×10^{-6} [44.5]	2.9×10^{-7} [44.2]
0.02	4.1×10^{-4} [14.3]	3.5×10^{-4} [56.1]	4.2×10^{-4} [36.6]
0.03	1.0×10^{-1} [4.5]	9.1×10^{-2} [7.1]	9.1×10^{-2} [4.6]
0.04	9.7×10^{-1} [2.2]	9.1×10^{-1} [3.3]	8.5×10^{-1} [2.3]
0.05	2.4 [2.0]	2.3 [2.7]	2.2 [1.8]
0.06	3.4 [2.1]	3.3 [2.7]	3.3 [1.7]
0.07	3.7 [2.3]	3.6 [2.8]	3.7 [1.8]
0.08	3.5 [2.2]	3.5 [2.9]	3.6 [1.8]
0.1	2.7 [2.5]	2.8 [3.2]	3.0 [2.0]
0.15	1.7 [2.8]	1.7 [3.5]	1.8 [2.2]
0.2	1.3 [2.9]	1.3 [3.5]	1.3 [2.2]
0.3	9.6×10^{-1} [2.9]	9.7×10^{-1} [3.6]	9.9×10^{-1} [2.2]
0.5	8.3×10^{-1} [2.9]	8.5×10^{-1} [3.7]	8.4×10^{-1} [2.4]
1.0	8.0×10^{-1} [3.4]	8.3×10^{-1} [4.4]	8.2×10^{-1} [2.7]
3.0	8.8×10^{-1} [3.8]	8.5×10^{-1} [4.7]	8.5×10^{-1} [3.0]
6.0	9.1×10^{-1} [3.6]	9.1×10^{-1} [4.3]	9.2×10^{-1} [2.7]
10.0	9.1×10^{-1} [3.2]	9.3×10^{-1} [3.8]	9.3×10^{-1} [2.4]

3.2. Simulation of coupled electron-photon transport

Table 3.8.: Jaw-averaged enamel DCCs, $C_{k,T}$, for the ISO-geometry at different locations. Shown in the brackets are values of the coefficient of variation (CV).

E (MeV)	Dose conversion coefficient $C_{k,T}$ (Gy Gy ⁻¹) [CV (%)]		
	Front	Front-Left and Front-Right	Left and Right
Buccal enamel			
0.01	6.0×10^{-4} [5.3]	5.8×10^{-4} [9.6]	4.8×10^{-6} [32.9]
0.015	5.1×10^{-2} [1.4]	4.4×10^{-2} [2.8]	6.4×10^{-3} [5.5]
0.02	3.1×10^{-1} [3.7]	2.6×10^{-1} [1.9]	9.0×10^{-2} [2.9]
0.03	1.5 [1.1]	1.3 [2.3]	7.4×10^{-1} [2.0]
0.04	2.8 [1.5]	2.5 [1.9]	1.7 [3.2]
0.05	3.6 [1.7]	3.3 [2.1]	2.5 [2.5]
0.06	3.7 [1.8]	3.5 [2.6]	2.8 [2.2]
0.07	3.4 [2.0]	3.3 [2.9]	2.9 [2.6]
0.08	3.0 [2.4]	2.8 [3.1]	2.7 [2.7]
0.1	2.2 [2.8]	2.2 [4.1]	2.1 [2.7]
0.15	1.2 [2.9]	1.2 [3.9]	1.3 [3.3]
0.2	9.4×10^{-1} [3.0]	9.3×10^{-1} [3.8]	9.4×10^{-1} [3.0]
0.3	7.5×10^{-1} [2.9]	7.4×10^{-1} [4.5]	7.3×10^{-1} [3.2]
0.5	6.7×10^{-1} [3.3]	6.7×10^{-1} [4.2]	6.3×10^{-1} [3.3]
1.0	6.6×10^{-1} [3.4]	6.6×10^{-1} [5.4]	6.3×10^{-1} [4.3]
3.0	7.2×10^{-1} [5.0]	7.3×10^{-1} [7.2]	6.7×10^{-1} [4.7]
6.0	6.9×10^{-1} [4.5]	6.9×10^{-1} [5.5]	7.0×10^{-1} [4.0]
10.0	6.4×10^{-1} [6.2]	6.5×10^{-1} [6.6]	6.9×10^{-1} [3.7]
Lingual enamel			
0.01	—	—	—
0.015	1.7×10^{-5} [39.5]	4.1×10^{-5} [59.7]	1.1×10^{-6} [36.1]
0.02	1.2×10^{-3} [22.9]	1.0×10^{-3} [54.1]	4.5×10^{-4} [40.8]
0.03	1.2×10^{-1} [5.8]	9.6×10^{-2} [8.2]	8.7×10^{-2} [7.7]
0.04	8.5×10^{-1} [3.2]	7.8×10^{-1} [4.6]	6.7×10^{-1} [3.1]
0.05	2.0 [2.7]	1.9 [4.1]	1.7 [3.1]
0.06	2.7 [2.9]	2.5 [3.6]	2.4 [2.7]
0.07	2.9 [3.1]	2.8 [4.5]	2.7 [3.2]
0.08	2.7 [3.1]	2.6 [4.6]	2.7 [3.2]
0.1	2.1 [3.4]	2.1 [4.6]	2.1 [3.1]
0.15	1.3 [4.5]	1.2 [5.5]	1.3 [5.3]
0.2	9.7×10^{-1} [3.8]	9.3×10^{-1} [4.8]	9.4×10^{-1} [3.5]
0.3	7.3×10^{-1} [3.5]	7.2×10^{-1} [5.4]	7.3×10^{-1} [3.1]
0.5	6.5×10^{-1} [4.0]	6.7×10^{-1} [5.6]	6.3×10^{-1} [3.7]
1.0	6.4×10^{-1} [4.7]	6.2×10^{-1} [5.8]	6.3×10^{-1} [5.3]
3.0	6.8×10^{-1} [5.5]	6.8×10^{-1} [7.8]	6.7×10^{-1} [6.2]
6.0	7.5×10^{-1} [5.2]	7.5×10^{-1} [6.9]	7.3×10^{-1} [4.8]
10.0	7.4×10^{-1} [5.7]	7.5×10^{-1} [9.5]	7.3×10^{-1} [4.1]

3. Results

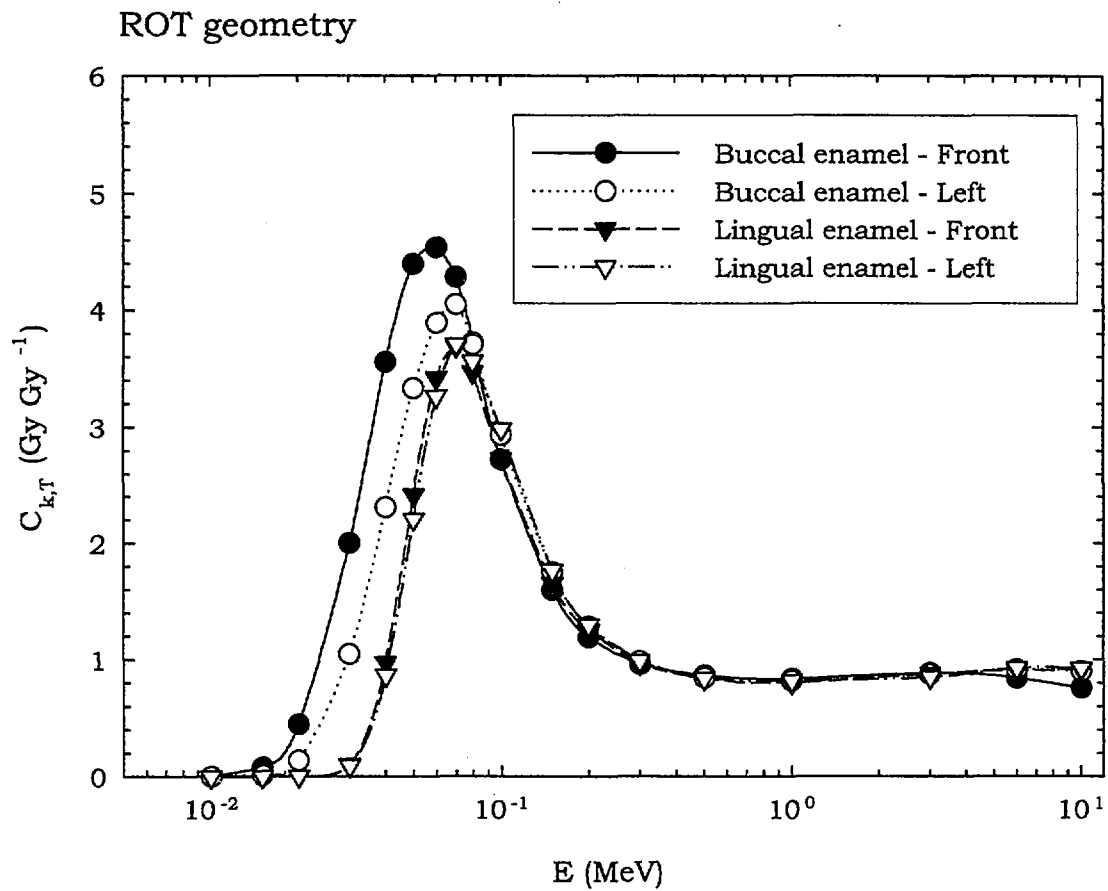


Figure 3.3.: Tooth enamel dose conversion coefficients for different locations/layers in ROT irradiation geometry. The coefficients are averaged over upper and lower jaws. Closed symbols location — «Front»; open symbols — location «Left».

3.2. Simulation of coupled electron-photon transport

Table 3.9.: Ratio of dose conversion coefficients for enamel and dentine computed without electron transport (kerma approximation) and with electron transport and electron energy cut-off equal to 10 keV. The data shown are for the «Front» tooth location under AP irradiation geometry. Shown uncertainties represent 2σ statistical errors.

E(MeV)	Ratio «kerma approximation/coupled transport»		
	Front buccal enamel	Front lingual enamel	Front dentine
0.3	0.999 ± 0.050	1.020 ± 0.067	0.992 ± 0.040
0.5	1.012 ± 0.035	1.006 ± 0.041	0.992 ± 0.028
1.0	0.985 ± 0.036	1.005 ± 0.042	1.004 ± 0.026
2.0	1.000 ± 0.039	1.033 ± 0.048	0.979 ± 0.031
10.0	2.051 ± 0.044	1.153 ± 0.058	1.318 ± 0.037

3. Results

4. Discussion

4.1. Comparison with other calculated data

Takahashi *et al.* [4, 5, 6] calculated and published dose conversion coefficients for the human tooth enamel. These data were computed using the EGS4 code with phantoms of two types. One phantom was a mathematical MIRD-type phantom of an adult, while the other was a voxel model of a physical phantom of a human head with authentic teeth. In both models the tooth region was split into five segments similar to the segmentation used in the present paper. Unlike the present work, Takahashi *et al.* did not separate between enamel and dentine and between buccal and lingual enamel regions. Instead, they calculated absorbed doses in the homogeneous whole teeth and rescaled the doses to obtain the dose coefficients for the enamel. The rescaling factor was the ratio of kerma coefficients for the enamel and the whole teeth materials.

Because of the apparent differences in the simulation techniques, the dose coefficients from Takahashi *et al.* and DCCs of the present work are not suited for direct comparison. Nonetheless, an attempt is made to compare the dose responses from [5] for AP and PA geometries for three different locations with DCCs for buccal and lingual enamel computed in the present study.

The comparison for the AP photon source is made in Fig. 4.1, from which one sees a good agreement between the data from Takahashi *et al.* for the whole teeth and the present dose conversion coefficients for buccal enamel in «Front» and «Front-Left» (corresponds to the location «Middle» of Takahashi *et al.*) locations. The coefficients for buccal enamel in «Left» location for energies of 50 and 80 keV are less than those of Takahashi *et al.* by 14 and 11%, correspondingly. The coefficients for the lingual enamel in the energy range from 20 to 100 keV are much lower than the DCCs for buccal enamel due to

4. Discussion

additional attenuation of the source photons and, consequently, different from those for the whole teeth of Takahashi *et al.*

Results of a similar comparison for the PA geometry are given in Fig. 4.2. The dose conversion coefficients for both buccal and lingual enamel are systematically lower by 10–20% than those of Takahashi *et al.* in the energy range above 200 keV and the difference becomes larger (up to 50% in «Front» and up to 30% in «Left» locations) at the energies less than 200 keV. These discrepancies can be explained by the above mentioned differences in computational procedures (rescaling), geometry of the target cells (whole teeth vs. buccal/lingual enamel), and, finally, from differences between phantoms (Golem vs. voxel and MIRD phantoms of Takahashi *et al.*)

4.2. Integral enamel dose and air kerma for occupational exposure scenarios

The enamel DCCs presented in the paper have been calculated primarily to support a reconstruction of occupational doses for the personnel of the Mayak reprocessing plant. Individual doses resulting from occupational exposure are estimated based on personal records of dosimetric data collected in different years and using different types of individual dosimeters. The dose reconstruction is a complicated and multi-stage process and validation of its results by independent methods is highly valuable. Human tooth enamel can be regarded as a personal dosimeter and the EPR-spectrometry of the tooth enamel can serve as an independent tool to validate individual doses derived from the personal dosimetric records.

The personal dosimeter readings, provided personal dosimeters calibration data, can be converted to organ doses and to integral air kerma in the working places. Thus, for validation of dosimetric data based on personal dosimetric records it is necessary to convert the tooth enamel dose to integral air kerma or to the organ doses. The conversion factors can be derived from Eqns. (2.8) – (2.10) assuming that the tooth absorbed dose is evaluated using the EPR-spectrometry: $D_T = D_{EPR}$. Then, the integral air kerma and the organ (or

4.2. Integral enamel dose and air kerma for occupational exposure scenarios

effective) dose are expressed through the measured tooth enamel dose:

$$K_a = c_a D_{EPR}, \text{ where } c_a = \frac{\int_E k_{tr}(E') \Phi(E') dE'}{\int_E C_{k,T}(E') k_{tr}(E') \Phi(E') dE'} \quad (4.1)$$

$$D_G = c_g D_{EPR}, \text{ where } c_g = \frac{\int_E C_{k,G}(E') k_{tr}(E') \Phi(E') dE'}{\int_E C_{k,T}(E') k_{tr}(E') \Phi(E') dE'} \quad (4.2)$$

It follows from eqns (4.1) and (4.2) that the conversion factors, c_a and c_g , depend on the energy distribution of photon fluence (photon spectrum) specific to a given workplace as well as on irradiation geometry and location of the tooth sample. In other words, if the tooth enamel is regarded as individual dosimeter then it must be remembered that this dosimeter has non-linear energy response; thus any conversion of tooth absorbed dose to integral air kerma or organ doses must account for energy distribution of the photon fluence.

An impact of fluence energy distribution is illustrated in the following example. The ratios of absorbed dose in various enamel layers and integral air kerma are calculated for AP and ROT geometries and four real-life photon spectra. These ratios are reciprocals of the conversion factors, and , in eqns (4.1) and (4.2) and shown in Table 11. The considered spectra include a standard A80 X-ray spectrum from Ankerhold (2000) and spectra for several workplaces in the Mayak reprocessing plant obtained by Vasilenko et al. (2000). Vasilenko et al. (2000) estimated energy distributions of photon fluence in spent-fuel storage of the Mayak plant in two locations (denoted P1 and P2) and on a bank of Karachay Lake, which was earlier used as storage for liquid radioactive waste. The fluences were derived by unfolding pulse-height spectra measured by a portable gamma-spectrometer with a high-purity germanium detector. The spectra do not extend beyond photon energy equal to 2 MeV. For the spectra from Vasilenko et al. (2000) a contribution to tooth absorbed dose from neutrons is assumed to be small and neglected. The ratio of neutron absorbed dose in tooth enamel and of air kerma appears to be of

4. Discussion

the order of 10^{-1} (Fattibene et al. 2002).

Table 4.1.: Ratio of absorbed dose in the different enamel layers and integral air kerma for various photon spectra and different tooth segments.

Spectra			Ratio $\frac{D_T}{K_a}$ ($Gy Gy^{-1}$) for							
			AP geometry				ROT geometry			
Name	Energy (MeV)		«Front»		«Left»		«Front»		«Left»	
	mean	median	B ^a	L ^b	B	L	B	L	B	L
A80 (X-ray) [22]	0.065	0.066	7.9	5.7	5.3	3.6	4.3	3.4	3.9	3.4
Karachay lake [9]	0.117	0.084	3.9	2.9	2.7	2.1	2.2	1.8	2.1	1.9
Storage-P1 [9]	0.226	0.134	2.0	1.8	1.7	1.4	1.4	1.3	1.4	1.3
Storage-P2 [9]	0.249	0.169	1.8	1.6	1.5	1.3	1.2	1.2	1.2	1.2

^aBuccal enamel

^bLingual enamel

Given in the Table 4.1 are also mean and median energies of the spectra. From the data in the table one can readily see that the tooth absorbed dose overestimates the air kerma. The overestimation ratio varies from 1.2 to 7.9 and shows a dependence on irradiation geometry, tooth location, enamel layer, and mean energy of the photon spectrum. The harder the spectra (i.e. the higher their mean energy) the lower is the value of the ratio. The highest overestimation ratios are obtained for soft X-ray spectrum.

The reconstruction of occupational doses for the personnel of the «Mayak» reprocessing plant using tooth doses derived by EPR-spectrometry requires a consideration of realistic energy-dependence of photon fluence at specific workplaces. That is, an application of the EPR-derived doses for reconstruction of integral air kerma values can be performed given specific exposure scenarios. Such scenarios should include the information on: (a) irradiation geometry and energy dependence of the photon fluence in a given workplace; and (b) personal working history, i.e. time spent at the given workplace. Having such exposure scenarios identified, the total individual occupational dose

4.2. Integral enamel dose and air kerma for occupational exposure scenarios

can be represented as a linear combination of dose responses to itemized scenarios.

4. Discussion

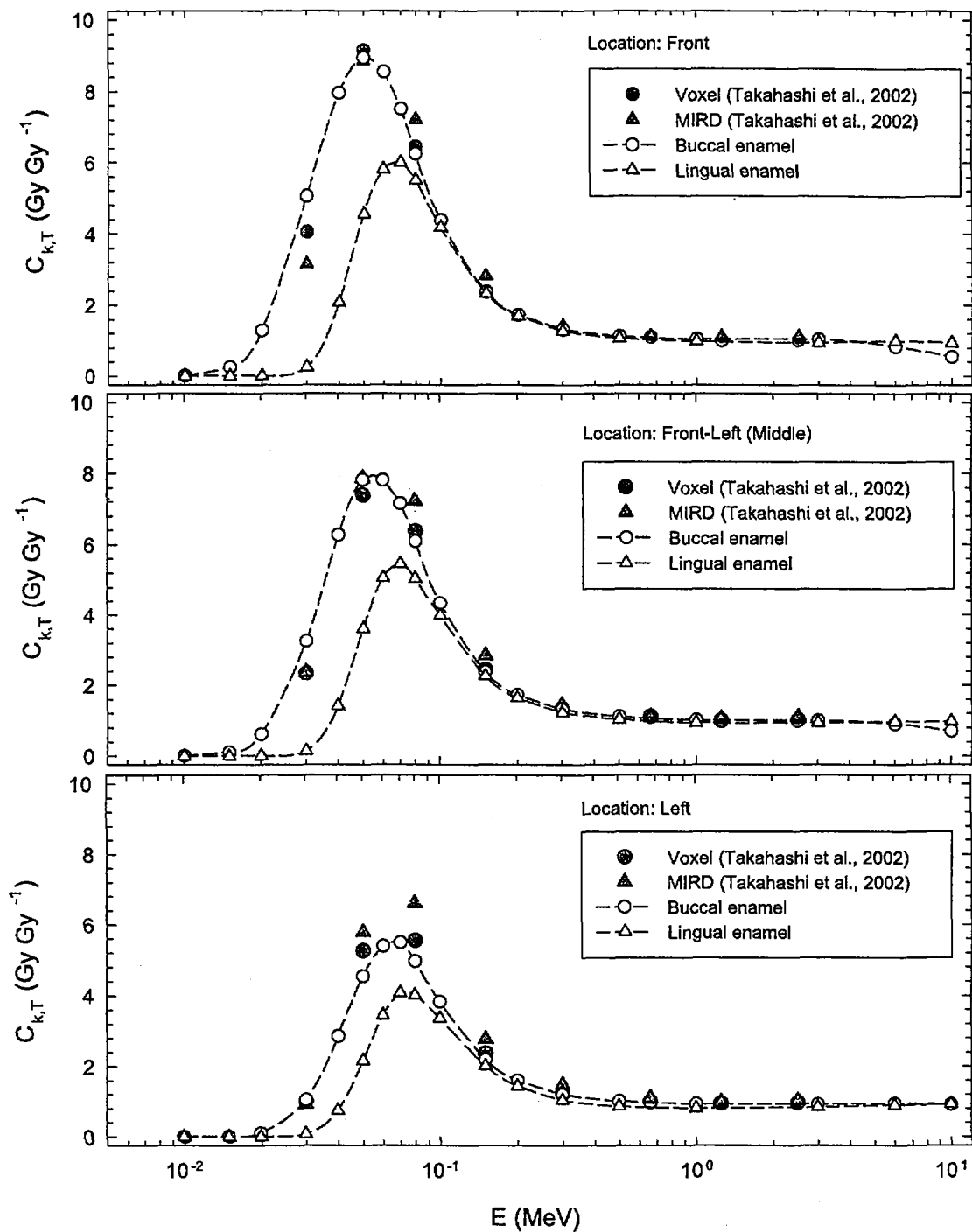


Figure 4.1.: Comparison of the dose conversion coefficients of the present study – open symbols, dashed line – for tooth enamel in AP irradiation geometry with those of Takahashi *et al.* [5] – closed symbols. Location «Front-Left» corresponds to location «Middle» in Takahashi *et al.* [5].

4.2. Integral enamel dose and air kerma for occupational exposure scenarios

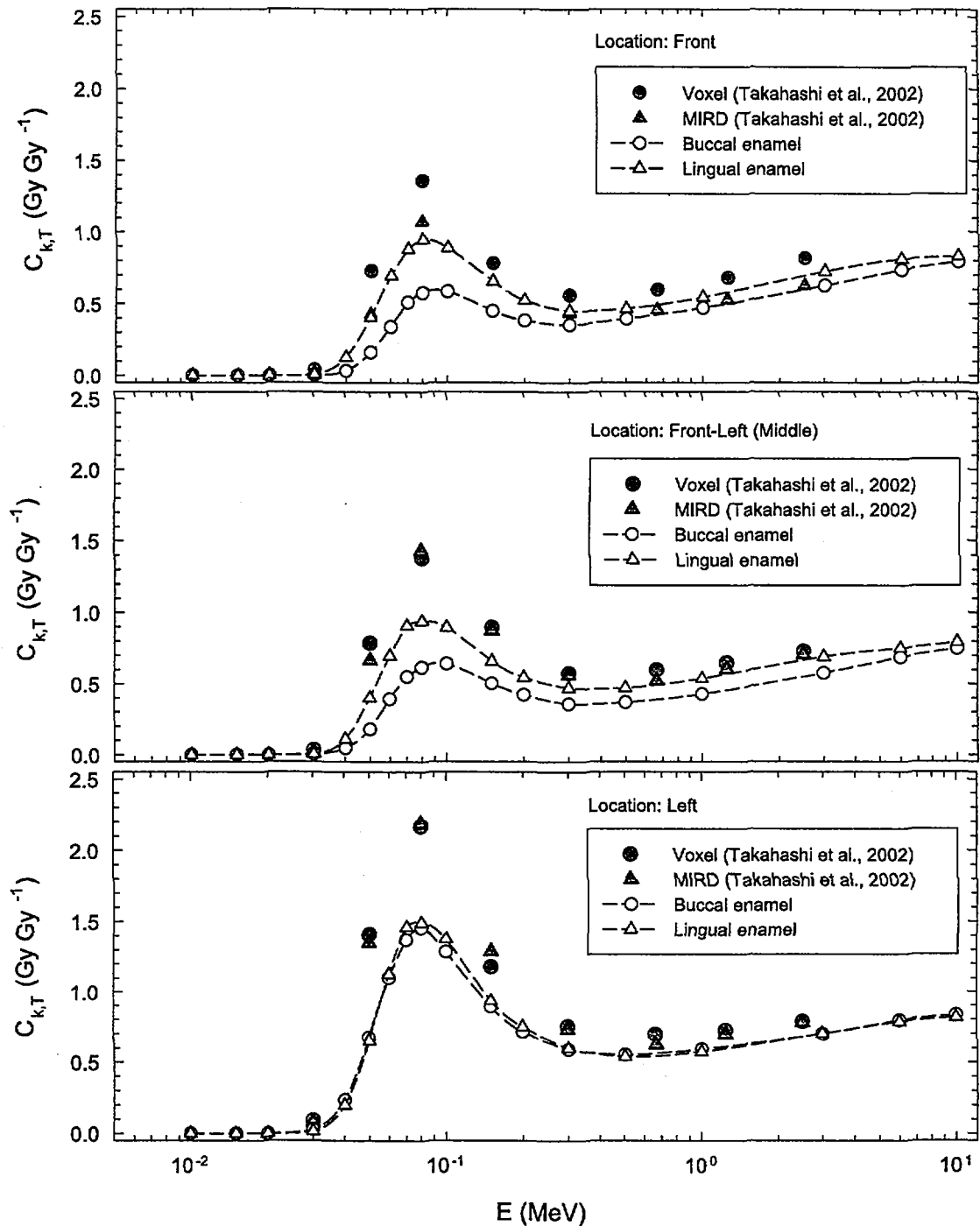


Figure 4.2.: Comparison of the dose conversion coefficients of the present study – open symbols, dashed line – for tooth enamel in PA irradiation geometry with those of Takahashi *et al.* [5] – closed symbols. Location «Front-Left» corresponds to location «Middle» in Takahashi *et al.* [5].

4. Discussion

5. Conclusions

Monte Carlo simulation of human teeth doses from photon sources of eight standard irradiation geometries has been performed and a set of dose conversion coefficients is calculated for 30 different tooth cells. The DCCs are presented as ratio of tooth absorbed dose to air kerma for monoenergetic photon sources. To facilitate handling of the data set a software utility has been developed. The utility plots the DCCs and computes conversion factors enamel dose air kerma and enamel dose organ dose for user-supplied discrete and continuous photon spectra.

The simulation illustrated that electron transport can be safely neglected in the Monte Carlo calculation of adult tooth enamel dose response to photons with energies less than 3 *MeV*. Photon spectra typical for environmental exposure (Karachay Lake) and for the spent fuel storage do not extend beyond 2 *MeV*, i.e. simulations for such spectra can be done in kerma approximation, which is more efficient computationally. However, this approximation might be inappropriate for other working places like a reactor hall or for teeth from children.

The computed dose conversion coefficients demonstrate non-linear energy dependence in the photon energy range from 0.02 to 0.2 *MeV*. Maxima of the energy dependence are observed in the range from 0.05 to 0.1 *MeV*. The energy dependence is stronger for monodirectional sources and locations with minimal shielding by non-tooth tissues, e.g. AP source and location «Front» or «RLAT» source and location «Right» and so on.

The tooth DCCs computed in the present work depend both on the location of a tooth sample and on the irradiation geometry. However, dependence on the sample location is generally weaker than that on irradiation geometry.

Comparison of the DCCs presented in the paper with those from other au-

5. Conclusions

thors has shown differences, especially, for low energies (below 100 keV) and strong attenuation of source photons (PA irradiation geometry). These differences can be attributed to differences in computational techniques and in the phantoms used in the studies. The observed discrepancies can be considered as representing uncertainties, caused by a variation of individual anatomical characteristics, in estimation of the tooth dose conversion coefficients, especially, in the low energy region where the impact of the phantom geometry is more influential.

Ratios enamel dose air kerma have been computed for several photon fluence spectra. Higher values of the ratios are for softer spectra, i.e. for those having lower mean energies. Among four spectra considered, the highest value of the ratio is obtained for the softest X-ray spectrum. This demonstrates a potential problem for individual dose assessment based on EPR-measurements of the teeth dose, namely, the lack of information on past medical X-ray exposure could lead to an overestimation of the individual dose.

The computed data will be used in occupational dose reconstruction problems, particularly ones related to the epidemiological study among workers in the Mayak reprocessing plant.

Acknowledgements

The Commission of European Communities under contract no. FIGD-CT-2000-00083 supported this work. Fruitful discussion with and suggestions made by Dr. Keith Eckerman (Oak Ridge National Laboratory, USA) are gratefully acknowledged.

5. Conclusions

Bibliography

- [1] International Atomic Energy Agency (2002) *Use of electron paramagnetic resonance dosimetry with tooth enamel for retrospective dose assessment*. Vienna: IAEA; IAEA-TECDOC-1331, ISBN 92-0-119402-1.
- [2] International Commission on Radiation Units and Measurements (2002) *Retrospective assessment of exposures to ionizing radiation*. International Commission on Radiation Units and Measurements: Bethesda, MD; ICRU Publication 68.
- [3] Wieser A, Aragno D, El-Faramawy N, Fattibene P, Meckbach R, Onori S, Presselo MC, Pugliani L, Ulanovsky A, Zankl M (2002) *Monte Carlo calculation and experimental verification of the photon energy response of tooth enamel in a head-sized Plexiglas phantom*. Radiation Protection Dosimetry 101: 549–552.
- [4] Takahashi F, Yamaguchi Y, Iwasaki M, Miyazawa C, Hamada T (2001) *Relations between tooth enamel dose and organ doses for the electron spin resonance dosimetry against external photon exposure*. Radiation Protection Dosimetry 95(2):101–108.
- [5] Takahashi F, Yamaguchi Y, Iwasaki M, Miyazawa C, Hamada T, Saito K (2002) *Conversion from Tooth Enamel Dose to Organ Doses for Electron Spin Resonance Dosimetry*, J. of Nuclear Science and Technology 39:964–971.
- [6] Takahashi F, Yamaguchi Y, Iwasaki M, Miyazawa C, Hamada T, Funabiki

Bibliography

- J, Saito K (2003) *Analysis of Absorbed Dose to Tooth Enamel against External Photon Exposure*, Radiation Protection Dosimetry 103(2):125–130.
- [7] International Commission on Radiological Protection (1996) *Conversion coefficients for use in radiological protection against external radiation*. Oxford: Pergamon Press; ICRP Publication 74.
- [8] Zankl M and Wittman A (2001) *The adult male voxel model "Golem" segmented from whole-body CT patient data*. Radiation and Environmental Biophysics 40:153–162.
- [9] Vasilenko EK, Smetanin MY, Knyazev VA, Slaughter M, Jacob P, David J, Feherbaher G (2000) *Approach to retrospective reconstruction of the photon exposure spectra at the technological sites of "Mayak" PA*. Radiation Safety Problems. Scientific Journal of "Mayak" PA 3:42–50. (In Russian)
- [10] International Commission on Radiation Units and Measurements (1992) *Measurement of dose equivalents from external photon and electron radiations*. International Commission on Radiation Units and Measurements: Bethesda, MD; ICRU Publication 47.
- [11] Hubbell JH, Seltzer SM (1995) *Tables of X-Ray Mass Attenuation Coefficients and Mass Energy-Absorption Coefficients (version 1.03)* [online]. Available: <http://physics.nist.gov/xaamdi>. Assessed 24 March 2003. National Institute of Standards and Technology, Gaithersburg, MD. Originally published as NISTIR 5632, National Institute of Standards and Technology, Gaithersburg, MD.
- [12] International Commission on Radiological Protection (1975) *Report of the Task Group on Reference Man*. Oxford: Pergamon Press; ICRP Publication 23.
- [13] Nelson WR, Hirayama H., Rodgers DWO (1985) *The EGS4 code system*. Stanford, CA: Stanford Linear Accelerator Center; Report SLAC-265.

- [14] Bielajew AF, Rogers DWO (1987) *PRESTA: parameter reduced electron-step transport algorithm for electron Monte Carlo transport*. Nuclear Instruments and Methods B18:165–181.
- [15] Fülle D, Wahl W (2003) *Modeling, simulation and measurement of radiation exposure using electronic personal dosimeters on realistic and ICRU phantoms*. Kerntechnik 68(4):130–134.
- [16] Kahn H (1956) *Use of different Monte Carlo sampling techniques*. In: Meyer HA, Ed. *Symposium on Monte Carlo methods*. New York: John Wiley and Sons.
- [17] Sobol IM (1973) *The Monte Carlo method*. Moscow: Nauka. (In Russian)
- [18] Carter LL, Cashwell ED (1975) *Particle transport simulation with the Monte Carlo method*. Oak Ridge, TN: Oak Ridge National Laboratory; USERDA Publication TID-26607.
- [19] Lux I, Koblinger L (1991) *Monte Carlo particle transport methods: neutron and photon calculations*. Boca Raton, FL: CRC Press.
- [20] Bell GI, Glasstone S (1970) *Nuclear reactor theory*. New York: Van Nostrand Reinhold.
- [21] Hudson DJ (1964) *Statistics. Lectures on elementary statistics and probability*. Geneva: CERN.
- [22] Ankerhold U (2000) *Catalogue of X-ray spectra and their characteristic data ISO and DIN radiation qualities, diagnostic and therapy radiation qualities, unfiltered X-ray spectra*. Braunschweig: PTB, Report PTB-Dos-34; ISBN 3-89701-513-7.

Bibliography

A. Appendix

A special-purpose software utility is written in the Python programming language to facilitate the handling of the computed data. The utility operates on a database of the results from the present Monte Carlo simulation. The data are stored as Python's dictionaries in separate files for each of eight geometries considered. Each file contains for 30 teeth cells the following data:

1. energy grid: 18 values in the energy range from 0.01 to 10 *MeV*;
2. computed dose per reference air kerma;
3. statistical uncertainty of the Monte Carlo estimate (2σ -values).

The utility has three main modes of operation:

- «Plot»;
- «Compute»;
- «Batch» (under development).

Common to the first two modes are panels for selection of irradiation geometry and the cell (see Fig. A.1). Irradiation geometries are represented by the eight standard geometries described in the paper. Data for can be selected from 30 basic teeth cells or they can be combined together to provide average over jaws, locations, inner/outer enamel layers. A possibility exists to compute average for the whole teeth region, also. Averaging between cells is done by weighting responses with masses of the respective cells.

In the «Plot» mode a user can visualize the dose coefficient for a specific cell (a group of cells). The data points are plotted and connected by cubic spline interpolating curve. Additionally, the user can save the plot in graphic PNG format or can save the data into a separate data table file in plain ASCII

A. Appendix

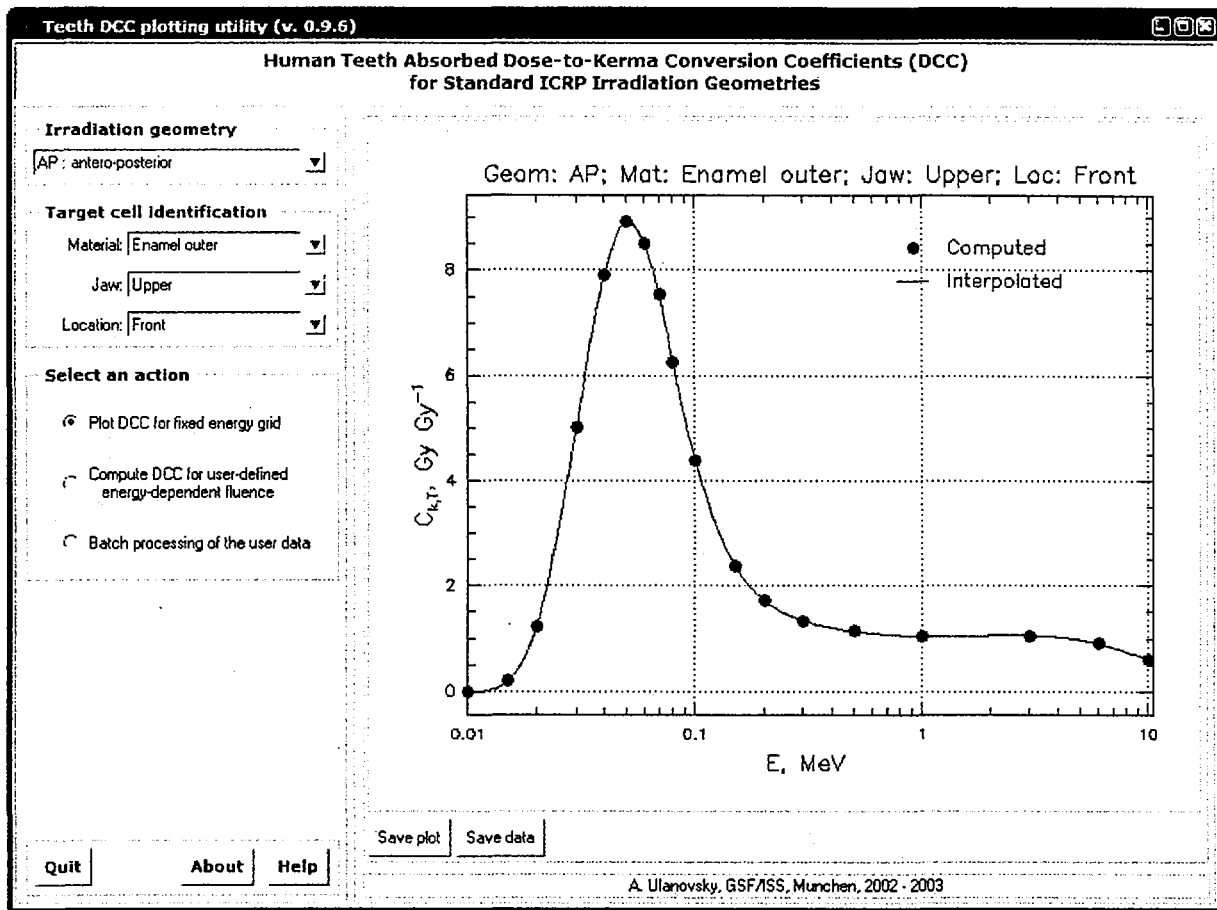


Figure A.1.: Screenshot of the utility in the operation mode «Plot».

format. An example of the utility operating in the «Plot» mode is shown in the Fig. A.1.

In the «Compute» mode (Fig. A.2) the utility can calculate teeth dose, air-kerma, and reference equivalent and effective doses using data from ICRP Publication 74 [7] according to Eqs. 2.8 – 2.10 for the user-supplied discrete or continuous normalized photon fluence. The photon fluence data can be input manually by the user into the special editing window or loaded from an external file. The fluence can be plotted as well (see Fig. A.3). If the user-supplied fluence data are to define a continuous spectrum then two interpolation options are available, namely, linear and cubic spline interpolation.

Scaling of the axis can be selected from linear or logarithmic. This scaling affects also a way of the energy-dependent fluence interpolation.

The third operation mode of the utility is «Batch» mode. Currently, it is under development. In this mode the utility will be capable of processing tooth sample data and output integral quantities (kermas and organ doses) for pre-defined radiation exposure scenarios and location of samples.

A. Appendix

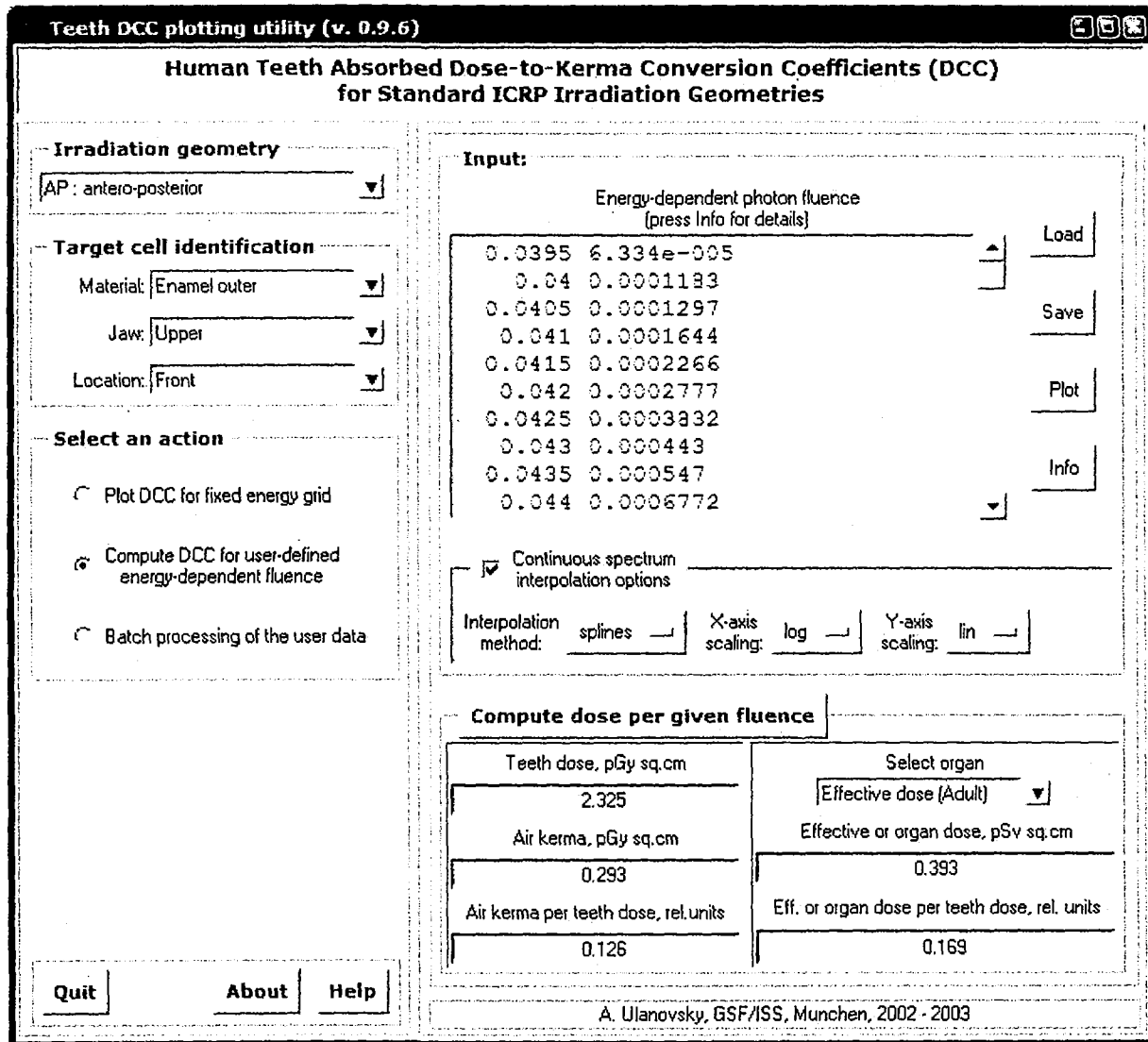


Figure A.2.: Screenshot of the utility in the operation mode «Compute».

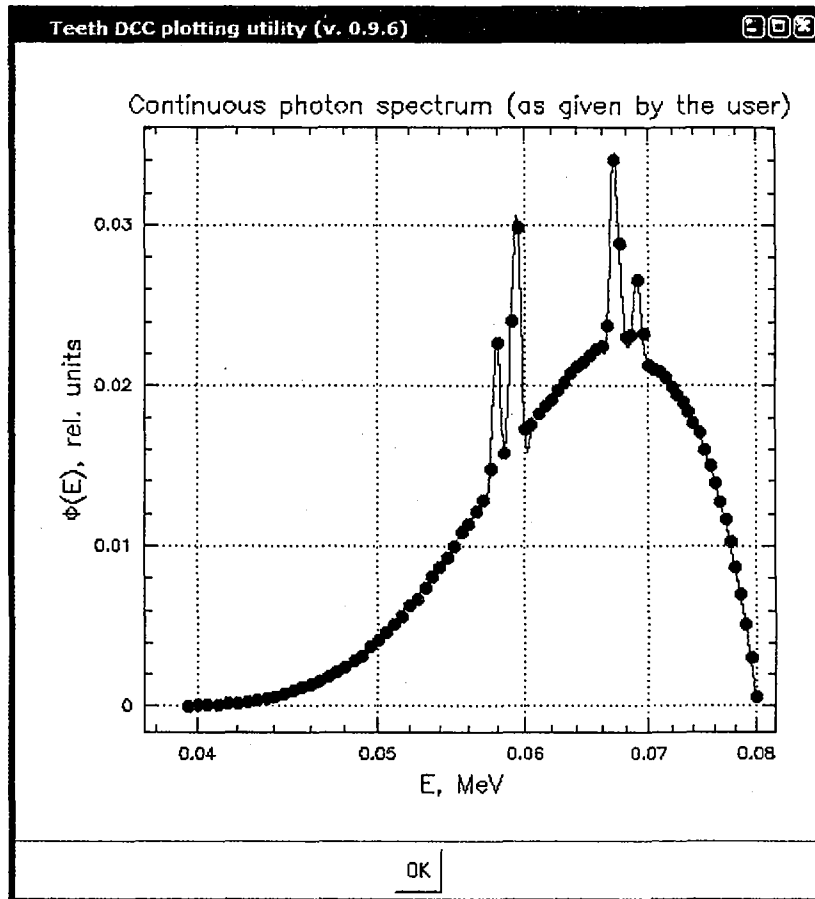


Figure A.3.: An additional window showing use-defined energy distribution of fluence. Shown is the A80 X-ray spectrum [22]. Options selected are: «x-log», «y-lin», and «spline interpolation».